FINAL REPORT, 1969

STIMULATED RAMAN EMISSION AND ABSORPTION SPECTROSCOPY

B.P. Stoicheff

University of Toronto
Departme t of Physics

Order No
NR 015-813/4-14-65

Code No.
5730K21

Contractor
The Governors
The University of Toronto

Date of Contract
1 June 1965 -

Amount of Contract
$111,142.00

Con.ract No.
Nonr-5012 (00) M-2

Expiration Date
31 August 1969

Project Scientist
Professor B.P. Stoicheff

Business
(416) 928-2948

Home
(416) 225-6421

TABLE OF CONTENTS

Introduction

The papers included in this final report describe in detail the research on stimulated Raman emission and absorption, as well as on normal Raman spectroscopy, carried out at the Department of Physics, University of Toronto in the period 1 June 1965 to 31 August 1969.

The main research centred on the comparison of experimental gain measurements with theory. Towards this end, materials were chosen in which the stimulated Raman effect was the dominant process. These included liquid O_2, N_2, and a crystal of diamond. The normal Raman linewidths were measured using He-Ne 6328 Å excitation and a Fabry-Perot spectrometer. Intensities of normal and stimulated Stokes radiation were measured and very good agreement with theory was obtained.

Several problems concerned with the angular distribution of Stokes and anti-Stokes radiation were undertaken. Diamond was found to be an ideal material for this study. Again, the results were in good accord with theory. Also, "surface" radiation in the Raman emission from filaments was observed in liquid mixtures and this showed the same angular distribution as Cerenkov radiation.

A brief study of the duration time and birefringence of filaments in liquid CS_2 was undertaken. Also, frequency

broadening by a short light pulse was investigated and explained by phase modulation of the intensity-dependent refractive index in filaments.

Techniques were also developed which may be of importance in Raman spectroscopy. Raman scattering in the forward direction was shown to be free from Doppler broadening and an effective resolution of $\sim 0.04\ cm^{-1}$ was achieved. This is a factor of 10 improvement over earlier work. High-speed Raman spectroscopy was shown to be possible using the inverse Raman effect and complete Raman spectra of liquids and solids were photographed in times as short as 40×10^{-9} sec.

FREQUENCY BROADENING IN LIQUIDS BY A SHORT LIGHT PULSE*

Fujio Shimizu†
Department of Physics, University of Toronto, Toronto, Canada
(Received 15 September 1967)

Several authors have reported the observations of frequency broadening in filaments which were produced by the self-focusing of a Q-switched laser in liquids.[1-3] This broadening has been attributed to the generation of new frequency components through an intensity-dependent refractive index and stimulated Rayleigh scattering.[1-4] Theories of the frequency broadening in an optical pulse by an intensity-dependent refractive index have been given in connection with the pulse distortion.[5,6] But comparison of experiment with theory has been difficult, because the broadening is usually irregular and the observation of the spectrum in filaments is obscured by the strong background. We report here the observation of the frequency broadening in a filament with short duration time, under such experimental conditions that the intensity of the stimulated Raman emission in the filament is much less than that of the laser. The structure of the frequency spectrum shows a pattern which can be explained by phase modulation through the intensity-dependent refractive index.

A Q-switched ruby laser beam with diameter 3 mm was used to produce filaments in a carbon disulfide liquid cell of 7.5 cm length. The intensity distribution of the light at the end of the cell was projected on the entrance slit of a spectrometer using a 5.2-cm focal-length lens with magnification of 17. In order to eliminate the nonscattered part of the laser beam from that in filaments, a wire with diameter of 1 mm was placed at the focusing point of the lens perpendicularly to the slit of the spectrometer. The entrance slit was wide open (about 2 mm). The resolution of the spectrum was determined from the magnitude of the image of the filament. The laser beam was composed of four or five groups of axial modes, the separation of the groups being approximately 0.45 cm^{-1}. With this mode structure the intensity of the laser beam changes considerably within the time interval $1/\Delta\nu$ where $\Delta\nu$ is the total spectral width. Therefore at relatively low laser power the duration time of the filament is expected to be 10^{-11} sec or less. (In the present experiments the laser power was kept lower than 50% above threshold for observations of optical trapping.) The total energy of a filament estimated from the photographic emulsion sensitivity is less than 10^{-7} J. Since the threshold for optical trapping in carbon disulfide is approximately 2 to 20 kW,[7] this energy also leads to a duration time of the order of 10^{-11} sec.

Typical spectra of the individual filaments in carbon disulfide are shown in Fig. 1. A regular periodic structure is observed in the low-frequency side of the broadening in every filament, when the broadening is smaller than the Raman shift. The period in a filament increases linearly with the amount of the broadening from the center. The average period for most filaments is 10 ± 3 cm^{-1} irrespective of the total magnitude of the broadening. The ratio between the intensity maxima and minima is at least 10. Most of the energy (about 90%) lies in the low-frequency side. The overall intensity is fairly uniform throughout the low-frequency side with an intensity maximum at the low-frequency extremity. In most cases an intensity peak is also observed at the laser frequency itself. A periodic structure but with larger spacing is also observed in the high-frequency side. The structure is smeared out when the low-frequency broadening is relatively large.

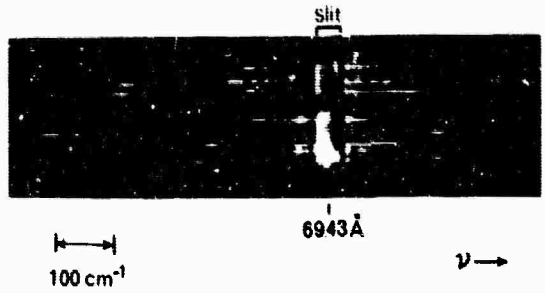

FIG. 1. Spectra of filaments in CS_2 excited with a single laser pulse. The vertical structure is produced by individual filaments occurring during the pulse. The frequency broadening (and periodic structure) is displayed in the horizontal direction and is evidently different for each filament. The image of the slit and the low-frequency side of the spectrum (at left) are attenuated by factors of 41 and 13, respectively, in comparison with the high-frequency side of the spectrum. (Some of the vertical fine structure within each filament is caused by diffraction by the masking wire placed at the focus of the objective lens.)

The regular periodic structure was usually observed only when the total spectral width of the laser radiation was fairly large. When filaments were produced by a laser with only two axial modes (separated by 0.8 cm^{-1}), the spectra of the filaments had a strong nonshifted center and were accompanied by a strong Raman Stokes spectrum. The structure in the spectrum was usually not as regular as observed in Fig. 1. When a single-mode laser was used, only a slight broadening was observed.

DeMartini et al.[6] have discussed pulse distortion by the intensity-dependent refractive index and have given examples of the numerical calculation of the frequency broadening where the distortion is fairly large. Since the amount of broadening in the present experiment is at most 5% of the laser frequency, we have treat the frequency broadening in the lowest order approximation neglecting the distortion of the intensity envelope. We will also discuss the mechanism of the periodic structure observed. The frequency broadening occurs through the phase modulation which is the result of the inhomogeneous phase velocity within a pulse. After a light pulse travels a distance L in the liquid, its phase is modulated by the intensity-dependent refractive index, as

$$\delta\varphi = (-k_0/n_0)L\delta n,$$

where k_0 is the wave vector of the initial laser beam in vacuum and δn is the change in the

refractive index given by

$$\delta n = \frac{n_2}{t}\int_{-\infty}^{t} dt' \langle E^2(t)\rangle e^{-(t-t')/\tau}.$$

In the above expression τ is the relaxation time and $n_2\langle E^2\rangle$ is the stationary value of the intensity-dependent refractive index. As an extreme case, if $\tau = 0$, the instantaneous frequency shift $d\delta\varphi/dt$ is proportional to $-d\langle E^2\rangle/dt$ and the frequency broadening occurs on either side of the center frequency. On the other hand, if τ is sufficiently large, $d\delta\varphi/dt$ is proportional to $-\langle E^2\rangle$ and the frequency broadening occurs only to the low-frequency side. The explanation of the periodic structure follows from a general consideration of a phase modulated wave. When the broadening is much larger than the inverse of the duration time of a pulse, the main contribution to the Fourier transform of $E(t)$, $\int E(t)\exp\{-i(\omega_0+\delta\omega)t\}dt$, at a particular angular frequency $\omega_0+\delta\omega$ comes from the integrals around the points at which the instantaneous frequency shift $d\delta\varphi/dt$ is equal to $\delta\omega$. For a pulse with a simple intensity envelope the condition $d\delta\varphi/dt = \delta\omega$ is satisfied at two points t_1 and t_2, for $\delta\omega < 0$. If we write values of integrals for these two parts as $I_1\exp(i\psi_1)$ and $I_2\exp(i\psi_2)$, respectively, the power spectrum is proportional to $I_1^2 + I_2^2 + 2I_1I_2\cos(\psi_2-\psi_1)$, where $\psi_2-\psi_1$ is expressed approximately by

$$\psi_2-\psi_1 \approx \{\delta\varphi(t_2)-\delta\varphi(t_1)\}-(t_2-t_1)\delta\omega.$$

The right-hand side of this expression is a steadily increasing function of $\delta\omega$ with positive second derivative. Therefore the interference term, $2I_1I_2\cos(\psi_2-\psi_1)$, produces a periodic structure in the spectrum with increasing spacing towards the low-frequency side. It can also be shown that the spectrum has its intensity maximum at the low-frequency extremity where the derivative of $d\delta\varphi/dt$ equals zero. If the pulse is symmetric, the minimum intensity in the periodic structure will be exactly zero. Although this is not the case for the pulses in Fig. 1, we may conclude that the pulse is not extremely asymmetric, because the observed ratio between the intensity maxima and minima is at least 10. The duration time of the filament is approximately the inverse of the average period in the low-frequency side, and is determined to be 6×10^{-12} sec. The high-frequency side can also be periodic, if τ is short enough compared with the duration time of the pulse.

In order to determine precisely the behavior of the broadening, more accurate measurements are necessary. Several factors, such as the temporal change in the intensity of the pulse and the deviation from the assumption of the simple relaxation time, which are not included in the above analysis, should be taken into account. A pulse with shorter duration time would be useful in order to study the dynamic behavior of the intensity-dependent refractive index in liquids.

It should be noted that among the liquids investigated (carbon disulfide, toluene, benzene, nitrobenzene, and mesitylene), the regular periodic patterns were observed in every filament in carbon disulfide only (also in some filaments in toluene). In all of these liquids, except carbon disulfide, a strong stimulated Raman emission was observed in each linear filament and the laser spectrum was either broad and irregular or very narrow. These observations can be explained if in carbon disulfide the laser pulse is not distorted appreciably by other nonlinear effects, such as stimulated Raman scattering, during the process of frequency broadening. In comparison with the other liquids, carbon disulfide has a large intensity-dependent refractive index (and the relaxation time for the relevant process is short). On the other hand, carbon disulfide has a relatively large gain for stimulated Raman scattering. However, this large gain is mainly due to the extremely narrow linewidth ($\sim$0.48 cm^{-1}).[8] When the stimulated Raman effect is excited by a pulse with a duration short compared with the relaxation time for the Raman process, the amplification is determined by the Raman cross section which is not so large in carbon disulfide compared with that in other liquids. Furthermore, since carbon disulfide has a large dispersion, the laser and Raman Stokes waves cannot long retain their favorable phase relation for maximum amplification of the Stokes wave. For these reasons, it is believed that distortion of the laser pulse is a minimum in carbon disulfide and results in the observed frequency broadening.

The author is greatly indebted to Professor B. P. Stoicheff for valuable discussions and for assistance with the manuscript and to Mr. A. K. McQuillan for assistance with some of the experiments.

*This research is part of Project DEFENDER under the joint sponsorship of the Advanced Research Projects Agency, the U. S. Office of Naval Research, and the Department of Defense. Also supported in part by the National Research Council, Canada.

†Postdoctorate Fellow, University of Toronto.

[1]R. G. Brewer, Phys. Rev. Letters 19, 8 (1967).

[2]Y. Ueda and K. Shimoda, Japan. J. Appl. Phys. 6, 628 (1967).

[3]H. P. H. Grieneisen and C. A. Sacchi, Bull. Am. Phys. Soc. 12, 686 (1967).

[4]N. Bloembergen and P. Lallemand, Phys. Rev. Letters 16, 81 (1966).

[5]R. J. Joenk and R. Landauer, Phys. Letters 24A, 228 (1967).

[6]F. DeMartini, C. H. Townes, T. K. Gustafson, and P. L. Kelley, to be published. T. K. Gustafson, F. DeMartini, C. H. Townes and P. L. Kelley, Bull. Am. Phys. Soc. 12, 687 P1967).

[7]R. H. Hellwarth, Phys. Rev. 152, 156 (1966).

[8]W. R. L. Clements and B. P. Stoicheff, private communication.

Angular Distribution of "Surface" Radiation in Stimulated Raman Scattering

Abstract—**Anti-Stokes emission in sharply defined cones has been observed from fine filaments in a mixture of acetone with 5 to 10 percent CS_2. The cone angle is in agreement with the momentum-matching condition that the longitudinal but not the transverse components sum to zero.**

The emission of anti-Stokes radiation during the stimulated Raman process is known to occur in two specific directional distributions which are strongly dependent on the experimental conditions. One type, the Class I distribution, has been observed in calcite,[1] in diamond,[2] and in several liquids[3] when suitable feedback of Stokes radiation is present, and is in good agreement with theory. A second distribution (Class II) has been observed in many liquids;[3]-[5] it occurs at larger angles than the Class I but is not well understood.

A distribution of anti-Stokes emission different from Class I and arising from "surface" radiation has been proposed by Szöke.[5] In stimulated Raman emission, "surface" radiation at the anti-Stokes frequency may be generated from laser and forward-directed Stokes radiation. The anti-Stokes emission is at an angle θ, given by the equation

$$k_1 \cos\theta = 2k_0 - k_{-1} \qquad (1)$$

where k_0, k_{-1} and k_1 are the wave vectors of the laser and first-order Stokes and anti-Stokes radiation. This relation implies that the longitudinal, but not the transverse, components of the phase velocities sum to zero,[4] a condition which could be satisfied when Stokes radiation is strongly directional and parallel to the incident laser wave,[6] as would be the case for Stokes radiation in a filament.

We report here the observation of "surface" radiation in stimulated Raman scattering with mixtures of acetone and carbon disulfide. We have observed first-order anti-Stokes emission in sharply-defined cones in the forward direction at the angle θ given by (1). At the same time, first-order Stokes radiation has been observed in very fine filaments produced by self-trapping of the radiation. The radiation used in these experiments was produced by a giant-pulse ruby laser. The laser pulses had a duration of ~40 ns, a power output of ~5 MW and a spectrum composed of one strong axial mode with one or two weaker modes. The liquids used were pure acetone and various concentrations of carbon disulfide in acetone, in cell lengths of 10 and 20 cm.

In pure acetone, usually only Class I distribution of anti-Stokes radiation was produced. An example of the far-field "ring" pattern is shown in Fig. 1(a). When a small amount (5 to 10 percent by volume) of carbon disulfide is added to acetone, the angular distribution is completely changed. Near threshold, it usually consists of a sharp ring (Fig. 1(c)) whose diameter is close to that of surface radiation given by (1). At higher excitation the sharp ring occurs together with a broad ring of smaller diameter (due to Class II radiation) as shown in Fig. 1(b). The half-angle θ of the sharp rings can be accurately determined and appears to vary slightly, from 6.5 to 6.8×10^{-2} rad, in different photographs taken with the 10 percent CS_2-acetone mixture. (The half-angle of the broad ring is $\sim 5.7 \times 10^{-2}$ rad.) According to (1) the angle θ is calculated to be 7.3×10^{-2} rad, based on the available data of the refractive index in this mixture.[7] (For pure acetone, (1) gives $\theta = 6.4 \times 10^{-2}$ rad.)

Similar experiments were carried out with cyclohexane, another liquid known to emit Class I radiation.[3] In mixtures with CS_2, again a sharp ring was observed, the measured emission angle being 6.8×10^{-2} rad for a 5 percent CS_2 mixture. Comparison with the angle for surface radiation, (1), was not possible since refractive index data for the mixture are not available, but for pure cyclohexane (1) gives 6.8×10^{-2} rad.

Near-field photographs taken at the exit end of the cell (Fig. 2) revealed the presence of filaments of laser, Stokes and anti-Stokes radiation in the CS_2-acetone mixtures, and their absence in pure acetone. Near threshold, the laser and Stokes filaments are of comparable intensity and occur with diameters of 20 to 100 μ. The corresponding anti-Stokes filaments appear to have smaller diameters, 8 to 16 μ; they are of higher intensity when they arise from the small diameter Stokes filaments; also the narrowness of the resulting rings indicates that the emission region is 1 to 2 mm long.

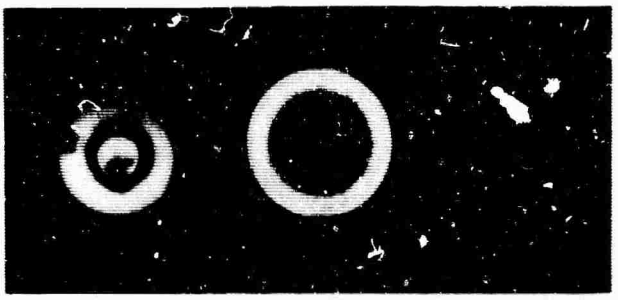

Fig. 1. Far-field "ring" patterns of anti-Stokes radiation in (a) pure acetone; (b) 10 percent CS_2-acetone mixture above threshold; (c) 10 percent CS_2-acetone mixture near threshold. There is no apparent difference in the spectral width (at $\Delta\nu = 2920$ cm^{-1}) of the anti-Stokes stimulated radiation in (b) and (c).

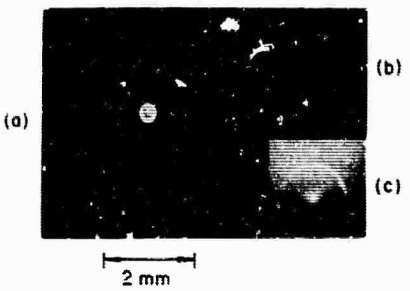

Fig. 2. Stimulated Raman emission from a 10 percent CS_2-acetone mixture. (a)(b)(c) photographed simultaneously. (a) Near-field photograph of anti-Stokes radiation showing filaments and associated "ring" patterns. The differences in ring diameters are due to the fact that the generating filaments occur at different distances from the exit window. (b) Near-field photograph of Stokes radiation (approximately the same magnification as (a)). A comparison of (a) and (b) shows that the anti-Stokes rings are generated from radiation in the filaments of smallest diameter. (c) Far-field photograph of anti-Stokes radiation.

Manuscript received March 22, 1968. This research is part of Project DEFENDER under the joint sponsorship of the Advanced Research Projects Agency, the U. S. Office of Naval Research, and the Department of Defense; it is also supported by the National Research Council, Canada, and the University of Toronto.

The total energy of Stokes radiation emitted from a small filament is estimated to be $\sim 10^{-6}$ joule, while the energy of anti-Stokes radiation is $\sim 10^{-3}$ joule. The observation of filaments thus satisfies the experimental condition necessary for generation of anti-Stokes radiation with the distribution given by (1). Moreover, with this information together with the gain in acetone[5] and the intensity-dependent refractive index of CS_2,[7] it can be shown that the fractional change of the wave vector due to the intensity-dependent refractive index would decrease the angle θ by about 10 percent, as observed.

The broad anti-Stokes rings are also emitted from filaments, but with Stokes radiation $\sim$100 times as intense as that of the filaments giving rise to the sharp anti-Stokes rings. They appear to be produced in a long emission region approximately 5 to 10 mm.

At the laser power levels used in the present experiments only stimulated radiation at $\Delta\nu = 2920$ cm^{-1} was observed in pure acetone and in the mixtures with CS_2; no stimulated radiation at $\Delta\nu = 656$ cm^{-1} due to CS_2 was detectable. The role of the CS_2 is simply to produce filaments.

From the present observations we conclude that the sharp anti-Stokes rings arise from "surface" radiation. Not only are their diameters in good agreement with the condition that only the longitudinal components of the phase velocities sum to zero, but they are also observed only in the presence of optical filaments in the liquid mixture.

F. Shimizu
U. Rachmann
B. P. Stoicheff
Dept. of Physics
University of Toronto
Toronto, Ontario, Canada

References

[1] R. Y. Chiao and B. P. Stoicheff, *Phys. Rev. Letters*, vol. 12, pp. 290–293, 1964.
[2] A. K. McQuillan and B. P. Stoicheff, *Bull. Am. Phys. Soc.*, vol. 12, p. 69, 1967.
[3] E. Garmire, *Phys. Letters*, vol. 17, pp. 251–252, 1965; P. L. Kelley, B. Lax, and P. E. Tannenwald, Eds., *Physics of Quantum Electronics*. New York: McGraw-Hill, 1966, pp. 167–179.
[4] P. D. Maker and R. W. Terhune, *Phys. Rev.*, vol. 137, pp. A801–818, 1965.
[5] A. Szöke, *Bull. Am. Phys. Soc.*, vol. 9, p. 490, 1964.
[6] K. Shimoda, *J. Appl. Phys.* (Japan), vol. 5, pp. 86–92 and 615–623, 1966.
[7] *International Critical Tables*, vol. 7. New York: McGraw-Hill, 1930, pp. 35, 78, 102.
[8] G. C. Bret and M. M. Denariez, *Appl. Phys. Letters*, vol. 8, pp. 151–152, 1966.
[9] G. Bisson, G. Bret, M. Denariez, F. Gires, G. Mayer, and M. Paillette, *J. Chim. Phys.*, vol. 64, pp. 197–208, 1967.

Reprinted from IEEE JOURNAL OF *QUANTUM ELECTRONICS*
Vol. QE-4, Number 6, June 1968
Pp. 425-426

Reprinted from
Volume 12, Number 8 APPLIED PHYSICS LETTERS 15 April 1968

RAMAN LINEWIDTHS FOR STIMULATED THRESHOLD AND GAIN CALCULATIONS*

W. R. L. Clements and B. P. Stoicheff
Department of Physics, University of Toronto
Toronto 5, Canada
(Received 19 February 1968)

Linewidths in the normal Raman spectra of several liquids of interest in stimulated Raman scattering have been measured including carbon disulfide, benzene, toluene, oxygen, and nitrogen. The spectra were excited with 6328-Å radiation from a He-Ne laser and examined with a pressure-scanned Fabry-Perot interferometer.

While it has long been known that Raman bands of totally symmetric vibrations exhibit extremely sharp lines even in liquids and solids, very few studies of the normal Raman effect have been concerned with accurate linewidth measurements. However, with the discovery of stimulated Raman scattering[1] there has been an increasing need for such measurements since both the threshold for stimulated scattering and the gain are dependent on the linewidths appearing in the normal Raman spectra. In the last few years, several linewidth measurements for liquids[2] and one for a solid[3] (calcite) have been reported, all making use of grating instruments. In the present Letter we describe a method for normal Raman linewidth measurements which is capable of even higher accuracy. Radiation at 6328 Å from a He-Ne laser is used for excitation of the spectra and a high-resolution Fabry-Perot interferometer for measurement. With this apparatus, linewidths of interest in stimulated Raman scattering have been measured for several liquids including carbon disulfide, benzene, toluene, oxygen, and nitrogen.

The experimental arrangement is shown in Fig. 1. It is based on the arrangement used by Chiao and Stoicheff[4] for Brillouin spectroscopy and is similar to systems used by Murray and Javan,[5] and Ducuing et al.[6] for Raman scattering with excitation by argon-ion lasers. In the present arrangement, the He-Ne laser has a power output of 150 mW and a linewidth of 0.025 cm^{-1} (full-width at half inten-

*This research is part of Project DEFENDER under the joint sponsorship of the Advanced Research Projects Agency, the U.S. Office of Naval Research, and the Department of Defense. Also supported by the National Research Council, Canada, and the University of Toronto.

sity). The 6328-Å radiation is isolated with a 10-Å band-pass filter and reflected into the sample cell. For the organic liquids the cell is a quartz capillary 2.5 mm in diam and 50 cm in length which acts as a light guide for the incident as well as for the scattered radiation. For liquid N_2 and O_2 the cell is a simple Dewar providing a scattering length of 7 cm between two flat windows. Raman radiation scattered in the backward direction is selected with a 100-Å band-pass filter and analyzed with a pressure-scanned Fabry-Perot interferometer. For CS_2, O_2, and N_2 the interferometer spacing was 2.950 mm; for N_2 a larger spacing of 9.943 mm was also used; for benzene and toluene the spacing was reduced to 0.869 mm in order to increase the spectral free range to 5.76 cm^{-1}. Pressure scanning with CO_2 from vacuum to 2 atm provided a chart of four interferometer orders when the 2.95-mm spacer was used. The measured instrumental width (made up of contributions from the laser width, Fabry-Perot response function for a reflectivity of 0.995, and the size of the detector aperture) is 0.050 cm^{-1} at 6328 Å and at almost all of the Raman wavelengths. At the wavelength of the N_2 Raman line (7423 Å) the mirror reflectivity decreased to 0.923 resulting in a calculated instrumental width of 0.063 cm^{-1} with the 2.95-mm spacer and 0.038 cm^{-1} with the 9.943-mm spacer.

In Fig. 2 is shown the 656-cm^{-1} Raman line of CS_2 in two adjacent orders. The line is relatively narrow and symmetric. It is superimposed on a broad background made up of overlapping of the wings of the line from different orders; in addition,

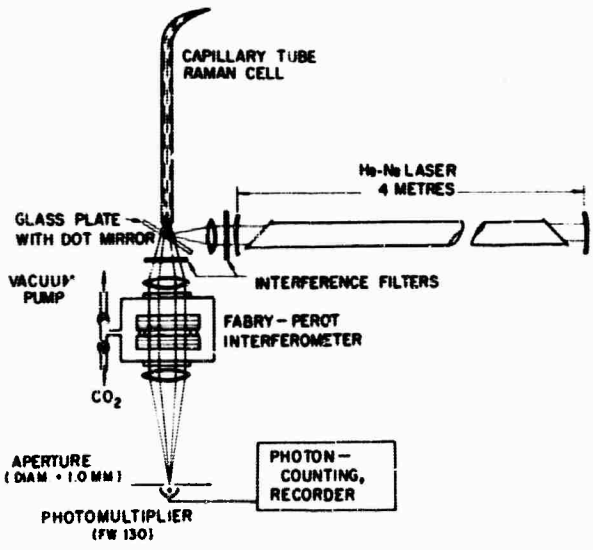

Fig. 1. Experimental apparatus for Raman linewidth measurements.

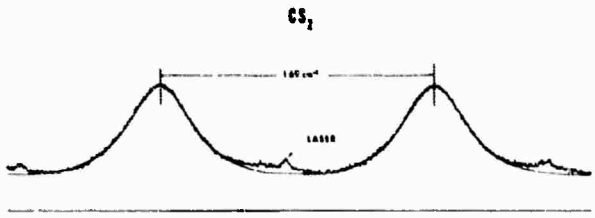

Fig. 2. Interferogram of the 656-cm^{-1} Raman line of liquid CS_2. Two adjacent orders are shown recorded with an interferometer spacer of 0.295 cm. The smooth line is the computed spectrum.

several nearby Raman lines (at 645.9 cm^{-1} due to $CS^{32}S^{34}$ and at 647.5, 652.7 cm^{-1} due to "hot" bands) contribute to the low intensity peak observed between the adjacent orders of the 656-cm^{-1} line. To determine the Raman linewidth the observed spectrum was compared with a computed spectrum obtained by assuming a Lorentzian line shape and convoluting this with the instrumental profile. Various Lorentzian linewidths were used in the calculations until good agreement between the observed and computed spectra was achieved taking into account the overlap of the different orders.

Similar computations were carried out for the most intense Raman lines in the several liquids studied here to obtain the values of full-width at half intensity listed in Table I. The estimated errors of the linewidths are approximately 5% of the measured widths although slightly larger for C_6H_6 and O_2. The 992-cm^{-1} line of C_6H_6 is the broadest of those observed and is slightly asymmetric due to overlapping by the much weaker lines at 983.6 cm^{-1} of $C^{13}C_5^{12}H_6$ and at 998.0 cm^{-1} of a "hot" band. The O_2 Raman line exhibited the lowest intensity of the liquids studied, since the laser radiation falls in the region of the strongest absorption band of liquid O_2.

The narrowest Raman line observed is that of liquid N_2, equal to 0.067 ± 0.004 cm^{-1}. Its intensity profile is shown in Fig. 3 where it is compared with

Table I. Linewidth Measurements of Totally Symmetric Vibrational Raman Lines.

Liquids	Raman Shift (cm^{-1})	Full-Width at Half Intensity (cm^{-1})
Nitrogen	2331	0.067 ± 0.004
Oxygen	1555	0.117 ± 0.008
Carbon disulfide	656	0.50 ± 0.02
Toluene	1002	1.94 ± 0.07
Benzene	992	2.15 ± 0.15

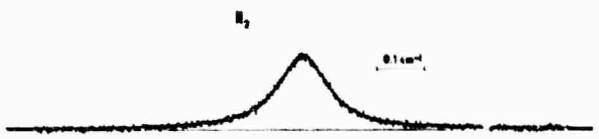

Fig. 3. Interferogram of the Raman line of liquid N_2 recorded with an interferometer spacer of 0.295 cm. The smooth line is the computed intensity profile.

that of the computed line. It may be noted that the same linewidth was obtained for both forward and backward scattering within the quoted experimental error. This value of the linewidth together with the relatively high intensity of the N_2 Raman line indicates perhaps one of the lowest thresholds for stimulated Raman emission and one of the highest gains.

The linewidth of 0.50 cm^{-1} obtained for liquid CS_2 is especially noteworthy in relation to the gain in stimulated Raman scattering. Although the recent literature[2] gives linewidths as narrow as 0.9, 1.0, and 1.4 cm^{-1}, the value usually used in gain calculations is 3 cm^{-1}. The present measurement shows that the linewidth is approximately 1/6 of this value and hence the gain is a factor of 6 larger than that quoted in the recent literature.[7]

In conclusion we should like to point out that not only does this method allow the accurate measurement of relatively narrow Raman lines in liquids (with possible extension to gases and solids) but it also provides a means of studying line shapes.

We are very grateful to G. I. A. Stegeman for the computer program used in the analysis.

[1] G. Eckhardt, R. Hellwarth, F. J. McClung, S. E. Schwarz, D. Weiner, and E. J. Woodbury, *Phys. Rev. Letters* **9**, 455 (1962).

[2] J. G. Skinner and W. G. Nilsen, *J. Opt. Soc. Am.* **58**, 113 (1968); F. J. McClung and D. Weiner, *J. Opt. Soc. Am.* **54**, 641 (1964); B. P. Stoicheff, *Phys. Letters* **7**, 186 (1963); N. I. Rezaev and R. Mezhetskii, *Opt. i Spektr.* **4**, 95 (1958); N. I. Rezaev and P. A. Bazhulin, *Opt. i Spektr.* **1**, 715 (1956).

[3] K. Park, *Phys. Letters* **22**, 39 (1966).

[4] R. Y. Chiao and B. P. Stoicheff, *J. Opt. Soc. Am.* **54**, 1286 (1964).

[5] J. R. Murray and A. Javan, *Bull. Am. Phys. Soc.* **12**, 113 (1967).

[6] J. Ducuing, A. P. Sheng, and J. R. Murray, private communication, 1966.

[7] G. Bisson, G. Bret, M. Denariez, F. Gires, G. Mayer, and M. Paillette, *J. de Chim. Phys.* **64**, 197 (1967).

BLANK PAGE

Reprinted from

PHYSICAL REVIEW VOLUME 180, NUMBER 1 5 APRIL 1969

Intensity and Gain Measurements on the Stimulated Raman Emission in Liquid O_2 and N_2*

J. B. Grun,† A. K. McQuillan,‡ and B. P. Stoicheff
Department of Physics, University of Toronto, Toronto 5, Canada
(Received 25 November 1968)

In liquid O_2 and N_2 the threshold for stimulated Raman emission is found to be much lower than for other nonlinear processes. Thus it is possible to make reliable measurements of the intensity of Raman emission over a large range of incident laser power by using a simple longitudinal geometry. Several distinct regions of emission were investigated, including normal Raman scattering, exponential gain, onset of oscillation, and saturation. There is good agreement with theory.

INTRODUCTION

It is well known[1-3] that the comparison of theoretical and experimental values of intensity and gain in stimulated Raman emission is complicated by several competing processes such as self-focusing, and Brillouin and Rayleigh scattering, all of which may have similar appearance thresholds. Thus, anomalous intensity behavior in many liquids and even in gases[4-6] and solids[7] appears to be the rule rather than the exception. One important consequence is that the premature onset of oscillation has precluded the observation of the expected exponential gain in most materials, with the exception of gaseous hydrogen, liquid acetone, and carbon tetrachloride.[8] Bloembergen and Lallemand[3,6] have overcome some of these difficulties by the use of a Raman amplifier and have demonstrated its importance in obtaining reliable values of the Raman gain. Other useful experimental arrangements in such studies include the transverse resonator of Dennis and Tannenwald,[9] the off-axis resonator of Jennings and Takuma,[10] and the diffusely pumped amplifier of Bortfeld and Sooy.[11] More recently, Shapiro, Giordmaine, and Wecht,[12] Bret and Weber,[13] and Kaiser and Maier[14] have shown that with picosecond and subnanosecond laser pulses stimulated Raman scattering is the dominant nonlinear scattering process in several liquids, and thus have obtained good agreement

with theoretical intensities.

The present investigation of laser stimulated Raman emission from liquid O_2 and N_2 arose from the results of earlier studies of the spectra of the normal and stimulated scattering. In one, it was shown that the linewidth of the normal Raman scattering was exceptionally narrow indicating a large Raman gain[15]; in another, concerning the stimulated Raman emission, extremely sharp spectral lines were observed (Fig. 1) without any evidence of broadening,[16] thus indicating that self-focusing and other scattering processes were not prominent. From these results we concluded that possibly the threshold for stimulated Raman scattering is lower than for the competing processes, in which case liquid O_2 and N_2 would be ideal substances for experimental study. Indeed, the present investigation has shown that liquid O_2 and N_2 are unique in this respect and no self-focusing or stimulated Brillouin scattering has been detected up to the highest incident laser power.

We wish to report our observations of the intensity of Raman Stokes radiation corresponding to the vibrational frequencies 1552.0 cm^{-1} and 2326.5 cm^{-1} of liquid O_2 and N_2, respectively. A simple longitudinal arrangement was used. The range of Raman intensity measurements includes the normal emission which varies linearly with incident laser power, a region of exponential gain over several orders of magnitude, the onset of oscillation with feedback by Rayleigh scattering and finally a region of saturation and depletion. The observed gain is in good agreement with that calculated from our experimentally determined cross-section for scattering.

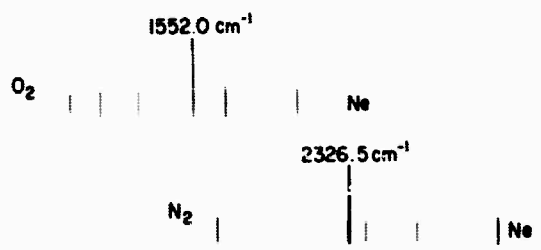

FIG. 1. Stimulated Raman spectra of liquid O_2 and N_2 showing the first-order Stokes vibrational lines at 1552.0 and 2326.5 cm^{-1}, respectively. The resolving power of the grating spectrograph is 10^5.

APPARATUS AND EXPERIMENTAL PROCEDURE

The exciting source was a giant-pulse ruby laser with a rotating prism at one end, and at the other a plane parallel reflector (~25% reflectivity) of Corning 2-58 glass which served as a mode selector[16] and also as a filter. The radiation was emitted in a single pulse of ~30-nsec duration and in a single (or nearly single) axial mode. Good reproducibility in the laser pulse was obtained by firing the laser at constant power near threshold, at regular (3 min) intervals with the ruby at a constant temperature (−10°C). This procedure also eliminated any spatial drift of the laser beam at the distant spectrometer slit.

The temporal behavior of a typical laser pulse is shown in Fig. 2(a). A study of the spatial intensity distribution of the laser beam was made at a magnification of 20× and by photographing the beam after attenuation by neutral density filters. This showed the presence of several intensity maxima [Fig. 3(a)] which increased the effective intensity of the laser beam to twice the average intensity. Also, the laser radiation was found to be plane polarized to better than 2000:1.

The longitudinal arrangement shown in Fig. 4 was used for the measurements of Raman scattering intensity and state of polarization in the forward direction. The sample container was a simple Dewar of 1 liter capacity with a path length of 5.8 cm between the two inner windows. It was positioned approximately 4 m from the laser in order to reduce possible feedback of scattered radiation to the laser. At each filling of the Dewar the liquid was passed through a 5μ millipore filter to remove any dust particles. A short time after a filling, the liquid became quiescent.

In order to increase the laser power density incident on the samples, the beam diameter was

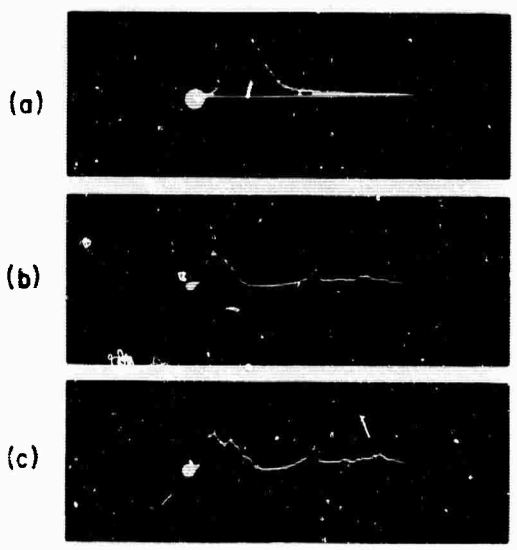

FIG. 2. (a) Typical laser pulse monitored with an ITT FW114A photodiode, and displayed on a Tektronix 519 oscilloscope. (b) Typical first-order Stokes pulse obtained in the saturation region, and the corresponding depleted laser pulse at the right. (c) Same as (b), but with the Stokes pulse also showing some depletion at higher laser power.

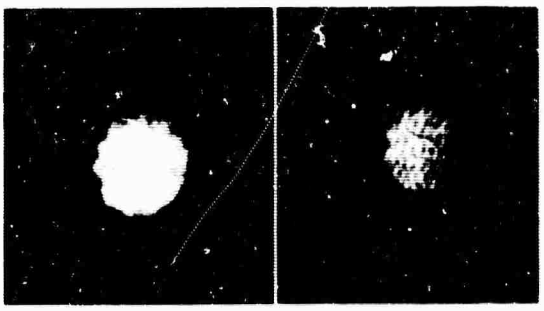

(a) (b)

FIG. 3. Near-field patterns showing the spatial intensity distribution of the incident laser beam (a) and the first Stokes emission (b), magnified 20×. Mottled appearance of Stokes picture is caused by laser attenuating filters.

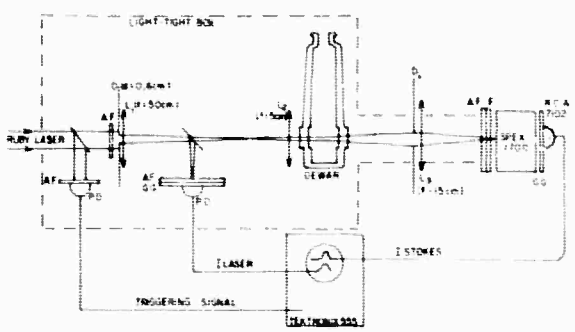

FIG. 4. Diagram of apparatus used for Raman intensity measurements. Explanation of symbols: *D* – diaphram, A. F. – attenuating filter, G. G. – ground glass, P. D. – E.G. & G photodiode (SGD-100), *L* – lens, *F* – filter.

reduced by a factor of about 10 (to 0.6 mm) with a system of two lenses. The incident laser power was varied from 30 kW to 600 kW by inserting calibrated neutral density filters of glass in the beam at the entrance diaphragm D_1 and lens L_1. The laser pulse was monitored with an EG & G photodiode (SGD-100), and displayed on a Tektronix 555 (or 519) oscilloscope. An essentially parallel laser beam was incident on the sample. The radiation scattered in the forward direction was collected through the exit diaphragm D_2 and focused on the slit of the spectrometer. The laser light entering the spectrometer was attenuated with calibrated filters. A grating spectrometer (Spex 1700) having a dispersion of 10 Å/mm was used with both entrance and exit slits open to 3 mm. Measurements of Stokes intensities were made with an RCA 7102 Photomultipler having a cooled photocathode (– 10°C). The signal was amplified 40 times by a two-stage emitter follower, and fed into a type *L* preamplifier of the oscilloscope. The pulse heights from the oscilloscope traces gave an effective measurement of the intensity of Stokes emission during each laser pulse. Brief studies of the laser and Stokes pulse envelopes were made with a fast photodiode (ITT FW 114A) and a Tektronix 519 oscilloscope. Depolarization measurements were carried out with a Nicol prism placed at the slit of the spectrometer.

Several precautions were taken to reduce any stray light and to minimize its effect on the intensity measurements, especially of the low-intensity normal Raman scattering. The main sources of unwanted stray light were found to be the laser flashlamp, and optical filters and lenses of glass along the laser beam which emitted relatively intense fluorescence radiation. Thus, all of the optics and sample Dewar were enclosed in a light-tight box having a 6 mm entrance aperture; diaphragms were placed along the laser beam path in front of lenses; and quartz lenses were used instead of glass lenses to minimize the fluorescence. Finally, the effects of the broad band fluorescence were suppressed by the use of a high-dispersion spectrometer.

For each liquid, the intensity measurements were carried out in two stages. In the low-intensity region of the normal Raman scattering, the light-collecting cone was 1.45×10^{-3} sr for N_2 and 5.80×10^{-4} sr for O_2. Calibrated filters were inserted in front of the spectrometer slit to cover the intensity range. In the high-intensity region of stimulated Raman emission the light-collecting cone was smaller, being 1.30×10^{-4} sr for both N_2 and O_2. Again, calibrated filters were used to make intensity measurements over approximately ten orders of magnitude. The laser pulse energy was measured with a calibrated thermopile (TRG 100). The many optical filters used to attenuate the laser and Raman radiation were calibrated spectrophotometrically (Beckman DU) each to an accuracy of 3%. The transmission characteristics of the spectrometer and the sensitivity of the photomultiplier were measured over the required wavelength region (and for light of parallel and perpendicular polarization) using a NBS standard lamp.

An estimate of the possible errors in making absolute intensity measurements of the Raman scattering indicated an accuracy of ±50%, the main source of error arising from the many filters used in attenuating the laser radiation. However the accuracy of relative intensity measurements was considered to be better than ±30%.

BRIEF RESUME OF THEORY

The theory of stimulated Raman scattering has been developed by many authors, notably, Hellwarth,[17] Bloembergen and Shen,[18] Townes and coworkers,[19] and Maker and Terhune.[20] They have

shown that the stimulated Stokes emission grows exponentially from noise according to the relation

$$I_S(l) = I_S(0)e^{+gll_0}. \quad (1)$$

Here, $I_S(l)$ is the intensity of the stimulated Stokes emission, $I_S(0)$ is the intensity of the normal (spontaneous) Stokes emission, I_0 is the incident laser power density, and l is the length of the amplifying medium. The gain g is given by

$$g = \frac{2c^2}{\pi h n^2} \frac{N}{\Delta\nu(\nu_0 - \nu_R)^3} d\sigma_{11}/d\Omega. \quad (2)$$

In general, and in the present work, g represents the gain for radiation polarized in the same plane as the incident plane-polarized laser radiation. In Eq. (2), c is the velocity of light, h is Planck's constant, n the refractive index, N is the effective number of molecules per cm^3, $\Delta\nu$ is the normal Raman linewidth, $\nu_0 - \nu_R$ is the frequency of the Raman line. The quantity $d\sigma_{11}/d\Omega$ is the total differential cross-section per molecule per sr for the one polarization, and may be evaluated from an absolute-intensity measurement of normal Raman scattering. Such a measurement gives the total differential cross-section for both polarized and depolarized scattering defined by[21]

$$\frac{d\sigma}{d\Omega} = \frac{2^4\pi^4}{c^4}\left(\frac{h}{8\pi^2\nu_R}\right)\frac{d}{\mu}(\nu_0 - \nu_R)^4 K\left(\frac{45\alpha'^2 + 7\gamma'^2}{45}\right) \quad (3)$$

for plane-polarized light incident on a system of randomly oriented molecules and observation in the scattering plane. Here ν_R is the frequency of the Raman-active molecular vibration, d is the degree of degeneracy of the vibration (=1 for the totally symmetric vibrations), μ is the reduced mass, and α' and γ' are, respectively, the isotropic and anisotropic parts of the derivative of the polarizability with respect to the internuclear coordinate at the equilibrium position. The constant K is the local field correction given by[22]

$$K = (n_S/n_0)(n_S^2 + 2)^2(n_0^2 + 2)^2/81, \quad (4)$$

where n_0 and n_S are the indices of refraction at the laser and Stokes frequencies, respectively. In order to evaluate γ' and α', it is necessary to measure the depolarization ratio

$$\rho = I_\perp/I_\parallel = 3\gamma'^2/(45\alpha'^2 + 4\gamma'^2).$$

Here $I_\perp$ and $I_\parallel$ are the intensities of scattered light polarized $\perp$ and $\parallel$, respectively, to the plane-polarized incident light.

It may be mentioned that Eq. (3) is valid only when the frequency of the incident exciting light is far from the main absorption bands of O_2 and N_2 which occur in the vacuum ultraviolet region.

EXPERIMENTAL RESULTS AND DISCUSSION

The observed intensity of first-order Stokes radiation over a range of incident laser intensity is shown in Fig. 5 for liquid O_2 and in Fig. 6 for liquid N_2. For both liquids, it was possible to investigate the Raman intensity over a range of approximately 12 orders of magnitude, from the very low intensity of normal scattering through a region of exponential amplification and oscillation to an intensity approaching the incident intensity, and finally saturation. These results will be discussed below under the headings (a) normal Raman scattering, (b) exponential gain, and (c) oscillation and saturation.

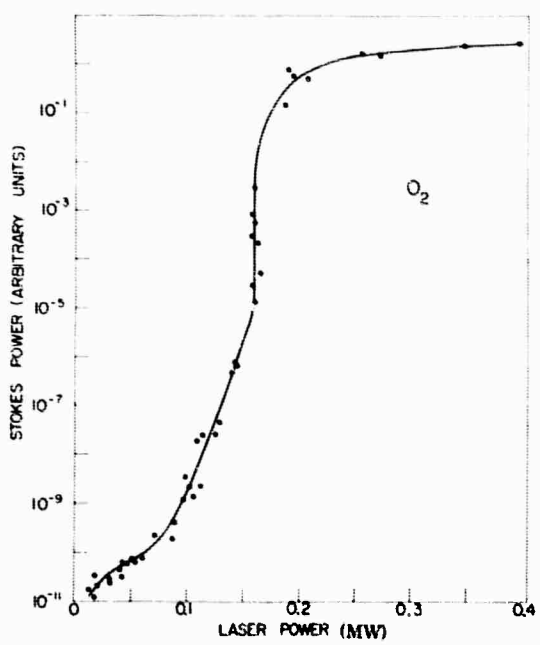

FIG. 5. Experimental curve for liquid oxygen showing Raman Stokes power as a function of incident ruby laser power.

(a) Normal Raman Scattering

The region of normal Raman scattering is one of very low intensity. Our measurements for O_2 and N_2 are given in Fig. 7. Although the data show considerable scatter, it is seen that there is a linear dependence of Raman intensity on incident laser intensity, as expected from theory. The slopes of the graphs of Fig. 7 were used to determine values of the differential scattering cross-section.

As already mentioned, the errors in making these absolute intensity measurements are approximately ±50%, whereas the accuracy of the relative measurements is perhaps ±30%. Thus the present

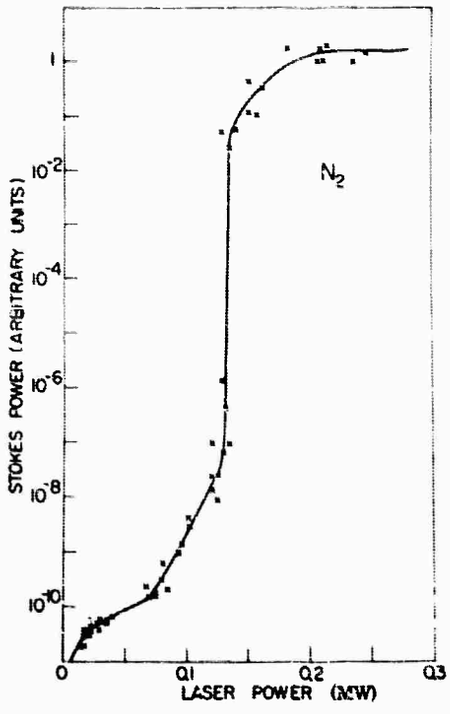

FIG. 6. Experimental curve for liquid nitrogen showing Raman Stokes output power as a function of incident ruby laser power.

TABLE I. Values of the total differential scattering cross-section for the 992 cm^{-1} Raman radiation of liquid benzene.

Authors	$d\sigma/d\Omega$ (10^{-30} cm^2 sr^{-1})	$d\sigma/d\Omega$ corrected for 6943 Å (10^{-30} cm^2 sr^{-1})
Damen, Leite, and Porto[23]	6.7 ± 1.2 (6328 Å)	4.5[a]
Skinner and Nilsen[24]	37.5 ± 4 (4880 Å)	4.95[b]
McClung and Weiner[22]	5.9 ± 3 (6943 Å)	5.9
Bret *et al.*[2]	9 (6943 Å)	9
Present authors	6.6 ± 3 (6943 Å)	6.6

[a]Calculated from $I\alpha(\nu-\nu_v)^4$, since the frequency of the exciting radiation ν is far from principal absorption frequencies. The Raman vibrational frequency is ν_v.

[b]Calculated from $I\alpha(\nu-\nu_v)^4/(\nu_a-\nu)^2$, since the frequency of the exciting radiation is near an absorption frequency ν_a.

method of determining the absolute Raman intensities was checked by measuring the scattering for the 992-cm^{-1} line of liquid benzene, and comparing the resultant value of the total differential scattering cross-section $d\sigma/d\Omega$ with values measured by other experimenters. This cross-section is related to experimentally measureable quantities by the equation

$$d\sigma/d\Omega = P_R/P_0 N l \Omega.$$

Here, P_R is the Raman power for the whole line scattered into the solid angle Ω and P_0 is the corresponding laser power, N is the density of molecules per cm^3 in the scattering medium, and l is the path length ($l = 10$ cm in our C_6H_6 experiment). Some of the recent values of $d\sigma/d\Omega$, for benzene are shown in Table I along with our value of $6.6 \pm 3 \times 10^{-30}$ cm^2 per molecule per sr. It is seen that the most accurate values are those obtained by Damen, Leite, and Porto[23] with a He-Ne laser and by Skinner and Nilsen[24] with an Ar^+ laser, which after correction for the ν^4 frequency dependence, are in very good agreement. We

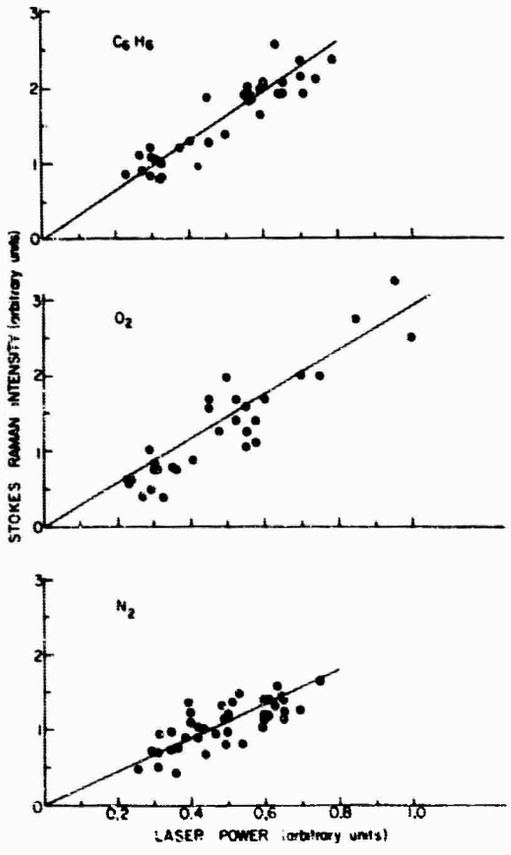

FIG. 7. Experimental measurements of normal Raman scattering for liquids, benzene, oxygen, and nitrogen. (Experimental scatter results from very low light levels used, necessitating a high amplification of the photomultiplier signal.)

have therefore taken the value $d\sigma/d\Omega = 4.50 \times 10^{-30}$ cm^2 for benzene (at $\lambda = 6943$ Å) as a basis for our evaluations, and have measured the ratio of the Raman intensities of the 2326-cm^{-1} line for N_2 and 1552-cm^{-1} line for O_2 relative to the 992 cm^{-1} for C_6H_6.

The results of these intensity measurements are given in Table II along with measurements of the depolarization ratio ρ for liquid O_2 and N_2. (We have also included values obtained for liquid CS_2.) The measured values of $d\sigma/d\Omega$ and of ρ were used to calculate values of $\alpha' = d\alpha/dr$, the rate of change of polarizability with nuclear displacement, from Eq. (3), after applying the local field correction K[Eq. (4)]. These are included in Table II. The values $\alpha' = 1.6 \times 10^{-16}$ cm^2 and 1.35×10^{-16} cm^2 for liquid N_2 and O_2, respectively, are the same as the values obtained for gaseous N_2 and O_2 by Stansbury, Crawford, and Welsh.[25] Our measured value of ρ for liquid N_2 agrees with that measured in the gas by Cabannes and Rousset,[23] but our value of ρ for O_2 is considerably lower than theirs.

(b) Exponential Gain

Under the present experimental conditions, the region of normal Raman scattering appears to hold up to incident laser powers of ~70 kW. At higher laser powers, both liquids exhibit regions of exponential gain, as shown by the linear portions of the graphs (plotted on semilog scales) in Figs. 5 and 6. For N_2 this region extends over a range of three orders of magnitude and for O_2, four orders of magnitude of Stokes amplification. These results represent stable regions of gain up to factors of at least e^6 and e^8 for liquid N_2 and O_2, respectively.

Values of the gain g(exp) were obtained from the slopes of the linear portions of the intensity curves (Figs. 5 and 6). These are given in Table III. Also listed for comparison are calculated values of the gain g(calc). The calculated values are based on the scattering cross-section $d\sigma/d\Omega$ evaluated here and on the linewidths 0.067 cm^{-1} for N_2 and 0.117 cm^{-1} for O_2 measured by Clements and Stoicheff,[15] making use of Eq. (2). It is seen that the values g(exp) and g(calc) are in good agreement.

(c) Oscillation and Saturation

For both liquids, the regions of exponential gain are abruptly terminated as shown by the discontinuity in slope of the Stokes intensity curves Figs. 5 and 6. These sharp changes in slope represent the onset of Raman oscillation with a rapid rise in output power. The oscillation threshold for N_2 occurs at somewhat lower laser power than for O_2; 0.13 MW compared with 0.16 MW for O_2. These values were not significantly affected by tilting the Dewar with respect to the incident laser beam or by the presence of ice particles in the liquids (although in the latter case the experimental error was greatly increased). The onset of oscillation is therefore not considered to arise from reflection at the windows or from scattering by

TABLE II. Values of the total differential cross-section, derivative of the polarizability and depolarization ratio.

Liquid	ν_p (cm^{-1})	$\frac{(d\sigma/d\Omega)\ \text{Liquid}}{(d\sigma/d\Omega)\ C_6H_6}$	$d\sigma/d\Omega$ (10^{-30} cm^2 sr^{-1})	α' (10^{-16} cm^2)	ρ
O_2	1552.0	0.056 ± 0.017	0.250 ± 0.075	1.35 (1.4)[b]	0.11 ± 0.01
N_2	2326.5	0.041 ± 0.012	0.185 ± 0.055	1.60 (1.6)[b]	0.10 ± 0.01
C_6H_6	992.2	1.00	4.5[a]	2.84	•••
CS_2	655.6	2.03 ± 0.60	9.1 ± 2.7	2.31	0.17 ± 0.02

[a]Value of Damen, Leite, and Porto[23] corrected for 6943 Å radiation.
[b]Values given by Stansbury, Crawford, and Welsh[25] for gaseous O_2, N_2.

TABLE III. Values of the Raman gain.

Liquid	$Nd\sigma_{\parallel}/d\Omega$ (10^{-8} cm^{-1} sr^{-1})	$\Delta\nu$[a] (cm^{-1})	g(calc) (10^{-2} cm MW^{-1})	g(exp) (10^{-2} cm MW^{-1})
O_2	0.48 ± 0.14	0.117	1.45 ± 0.4	1.60 ± 0.50
N_2	0.29 ± 0.09	0.067	1.70 ± 0.5	1.60 ± 0.55
C_6H_6	3.06	2.15	0.28	•••
CS_2	7.55	0.50	2.4	•••

[a]Values of linewidths measured by Clements and Stoicheff.[15]

bubbles, dust, or ice particles. Also, we have experimentally ruled out the possibility that the rapid rise in output power is caused by self-focusing. Near-field photographs of the laser and Stokes radiation at the exit window show no evidence of filament formation and uniform Stokes emission over the beam cross-section [Fig. 3(b)]. No filaments were observed up to the highest laser power used 1 MW, where the self-focusing length is calculated to be 5 cm for O_2 and 9 cm for N_2. The critical power for self-focusing[27,28] calculated from the known Kerr constants[29] is 200 kW for O_2 and 600 kW for N_2. The observed onset of oscillation occurs at lower laser powers as mentioned above. Moreover, the ratio of laser power at threshold of oscillation in O_2 to that in N_2 was measured to be 1.20 ± 0.006 as compared with the ratio of 0.3 for the respective critical powers for self-focusing.

We believe that the most likely cause of oscillation is feedback of Stokes radiation scattered in the backward direction by Rayleigh scattering. This is suggested by the high Raman gain for these liquids and by the ratio of 1.2 for the gain constants of O_2 and N_2, which is the same value as the ratio of laser power for oscillation. The Rayleigh scattering intensity determined by Stansbury, Crawford, and Welsh[25] for gaseous O_2 and N_2, together with the local field factor for the liquids, leads to a feedback factor of $Nd\sigma/d\Omega$ (Rayleigh) $= 6.1 \times 10^{-6}$ per cm per unit solid angle for liquid N_2 and 6.6×10^{-6} units for O_2. For the effective solid angle of our experiments ($\sim 10^{-4}$ sr) the feedback factor is approximately 10^{-5} per cm, which is sufficient to explain the onset of oscillation.

In the region of oscillation the rise in Stokes intensity is very steep, and represents an increase of five orders of magnitude for liquid O_2 and seven orders of magnitude for liquid N_2.[6,30] The uppermost portions of the intensity curves (Figs. 5 and 6) are similar, and indicate strong depletion of laser radiation and conversion to Stokes radiation. The oscilloscope trace in Fig. 2(b) shows a typical pulse of Stokes radiation in this region with the corresponding laser pulse severely distorted. This process results in the flat tops of the intensity curves and is the region of saturation. At still higher incident laser powers, the first-order Stokes radiation is converted to second-order Stokes (and anti-Stokes radiation) which results in depletion of the first-order Stokes intensity. This depletion is shown in the oscilloscope trace of Fig. 2(c).

A brief study of the conversion of laser radiation to first-order Stokes radiation for liquid N_2 was carried out, and the results are presented in Fig. 8. Here is plotted the ratio P_{out}/P_{in}, normalized for the laser radiation. The general behavior of this ratio is in good agreement with the theory of Shen and Bloembergen.[18] Figure 6 shows high conversion of approximately 75% laser radiation to first-order Stokes radiation in the saturation region.

CONCLUSION

This experiment has shown that liquid N_2 and O_2 are important materials for the study of stimulated Raman scattering. Because of their high Raman gain, the stimulated Raman effect emerges as the dominant nonlinear process in these liquids. Thus it was possible to investigate the intensity characteristics and build-up of Stokes radiation over a range of 12 orders of magnitude; from the low-intensity normal scattering through exponential amplification, oscillation and saturation, and eventual depletion. A detailed study of the region of normal scattering and exponential gain shows very good agreement with theory. The regions of higher intensity also reveal the expected theoretical behavior and warrant closer study. Finally the high conversion efficiency of laser to Raman Stokes radiation indicates that these liquids are very useful as new frequency sources.

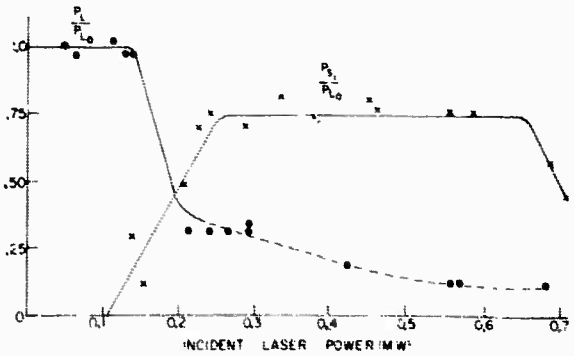

FIG. 8. Experimental curves showing how the ratios of the laser power (P_L) and the first Stokes power (P_s) at the exit of the Dewar, to the incident laser power (P_{L0}), vary with the incident laser power. The dashed curve in the depleted laser region is only approximate as the laser pulse was severely distorted.

ACKNOWLEDGMENT

We are very grateful to Dr. Fujio Shimizu for many helpful discussions.

†This research is part of Project DEFENDER under the joint sponsorship of the Advanced Research Projects Agency, the U.S. Office of Naval Research, and the Department of Defense. Also supported by the National Research Council, Canada, and the University of Toronto.

*On leave from Laboratoire de Spectroscopie, Université de Strasbourg, France.

‡Holder of Province of Ontario Government Scholarships 1965–68.

[1]J. F. McClung, W. G. Wagner, and D. Weiner, Phys. Rev. Letters 15, 96 (1965); in Physics of Quantum Electronics, edited by P. L. Kelley, B. Lax, and P. E. Tannenwald (McGraw-Hill Book Company, Inc., New York, 1966), pp. 155–158.

[2]G. Bret, Compt. Rend. 259, 2991 (1964); 260, 6323 (1965), G. Bret and G. Mayer, in Physics of Quantum Electronics, edited by P. L. Kelley, B. Lax, and P. E. Tannenwald (McGraw-Hill Book Company, Inc., New York, 1966), pp 180–191; G. Bisson, G. Bret, M. Denariez, F. Gires, G. Mayer, and M. Paillette, J. Chim. Phys. (Paris) 64, 197 (1967).

[3]P. Lallemand and N. Bloembergen, Appl. Phys. Letters 6, 210, 212 (1965): in Physics of Quantum Electronics edited by P. L. Kelley, B. Lax, and P. E. Tannenwald (McGraw-Hill Book Company, Inc., New York, 1966), pp. 137–154.

[4]R. W. Minck, E. E. Hagenlocker, and W. G. Rado, Phys. Rev Letters 17, 229 (1966).

[5]G. Bret and M. Denariez, Phys. Letters 22, 533 (1966).

[6]N. Bloembergen, G. Bret, P. Lallemand, A. Pine, and P. Simova, IEEE J. Quantum Electron. QE-3, 197 (1967).

[7]G. Bisson and G. Mayer, J. Phys. 29, 97 (1968).

[8]G. Bret and M. Denariez, J. Chim. Phys. (Paris) 64, 222 (1967).

[9]J. H. Dennis and P. E. Tannenwald, Appl. Phys. Letters 5, 58 (1964)

[10]D. A. Jennings and H. Takuma, Appl. Phys. Letters 5, 239 (1964).

[11]D. P. Bortfeld and W. R. Sooy, Appl. Phys. Letters 7, 283 (1965).

[12]S. L. Shapiro, J. A. Giordmaine, and K. W. Wecht, Phys. Rev. Letters, 19, 1093 (1967).

[13]G. Bret and H. P. Weber, IEEE J. Quantum Electron. QE-4, 28 (1968).

[14]W. Kaiser and M. Maier, IEEE J. Quantum Electron. QE-4, 67 (1968); private communication (1968).

[15]W. R. L. Clements and B. P. Stoicheff, Appl. Phys. Letters 12, 246 (1968).

[16]B. P. Stoicheff, Phys. Letters 7, 156 (1963); Quantum Electronics and Coherent Light, Proceedings of the International School of Physics "Enrico Fermi," Course XXXI, 1963, edited by C. H. Townes and P. A. Miles (Academic Press, Inc., New York, 1964), pp. 306–325.

[17]R. Rellwarth, Phys. Rev. 130, 1850 (1963); Current Sci. (India) 3, 129 (1964).

[18]N. Bloembergen and Y. R. Shen, Phys. Rev. 133, A37 (1964); 137, A1787 (1965).

[19]E. Garmire, E. Pandarese, and C. H. Townes, Phys. Rev. Letters, 11, 160 (1963); R. Y. Chiao, E. Garmire, and C. H. Townes, in Quantum Electronics and Coherent Light, Proceedings of the International School of Physics "Enrico Fermi," Course XXXI, 1963, edited by C. H. Townes and P. A. Miles (Academic Press, Inc., New York, 1964), pp. 326–338.

[20]P. D. Maker and R. W. Terhune, Phys. Rev. 137, A801 (1965).

[21]G. Placzek in Handbuch der Radiologie (Akademische Verlagsgesellschaft, Leipzig, Germany, 1934), Vol. VI, Pt. 2, pp. 205–274.

[22]G. Eckhardt and W. G. Wagner, J. Mol. Spectry. 19, 407 (1966).

[23]T. C. Damen, R. C. C. Leite, and S. P. S. Porto, Phys. Rev. Letters 14, 9 (1965).

[24]J. G. Skinner and W. G. Nilser, J. Opt. Soc. Am. 58, 113 (1968).

[25]E. J. Stansbury, M. F. Crawford, and H. L. Welsh, Can. J. Phys. 31, 954 (1953).

[26]J. Cabannes and A. Rousset, Compt. Rend. (Paris) 206, 85 (1938).

[27]R. Y. Chiao, E. Garmire and C. H. Townes, Phys. Rev. Letters 13, 479 (1964).

[28]P. L. Kelley, Phys. Rev. Letters. 15, 1005 (1965).

[29]R. Guillien, Physica 3, 895 (1963).

[30]cf. P. V. Avizonis, K. C. Jungling, A. H. Guenther, R. M. Heimlich, and A. J. Glass, J. Appl. Phys. 39, 1752 (1968).

A Study of the Duration and Birefringence of Self-Trapped Filaments in CS_2*

Fujio Shimizu† and B.P. Stoicheff
Department of Physics
University of Toronto
Toronto, Canada

Small-scale optically-trapped filaments in liquid CS_2 were studied by side illumination and crossed polarizers using the second harmonic radiation of a mode-locked Nd^{3+}:glass laser. Filaments produced by Nd^{3+} laser radiation (1.06 μ) exhibited birefringence of magnitude $(2\pm1)\times10^{-3}$ and duration times $< 10^{-11}$ sec.

A Study of the Duration and Birefringence of Self-Trapped Filaments in CS_2*

Recent experimental investigations of optically-trapped small-scale filaments[1] in liquids have given valuable information on properties such as threshold power, focusing length, energy, and diameter of filaments. However, other fundamental quantities such as duration time and refractive index changes remain uncertain, mainly because of the difficulty of making direct measurements during the short duration time of the filaments[2-4]. We report here on the photographic investigation of filaments in liquid CS_2 illuminated from the side by second-harmonic radiation of a mode-locked Nd:glass laser[5] and observed through crossed polarizers. Such experiments can give direct information about the refractive index changes in filaments and also about their duration time, provided the time is much shorter than the travelling time of the light in the liquid sample.

In the present investigation, filaments were produced by either 1.06 μ or 0.694 μ radiation from mode-locked lasers of Nd:glass or ruby, respectively. The Nd:glass laser emitted a train of 20 pulses with pulse duration ~ 6 psec as determined by double-photon fluorescence ; the ruby laser emitted fewer pulses and with duration times $<$ 0.2 nsec. The main laser radiation producing the filaments was directed along the length of a rectangular sample cell. For analysis of the filaments, a second and less intense laser beam was transmitted from the side of the cell, at right angles to the main laser beam and coincident with it in the sample.

This was a collimated beam of 0.53 μ (second-harmonic) radiation from the mode-locked Nd:glass laser. When 1.06 μ radiation was used to produce filaments, the same Nd laser provided the radiation for filament formation and for side illumination: when 0.694 μ radiation was used to produce filaments, synchronization of the ruby and Nd laser pulses was achieved by switching the Kerr-cell Q-spoiler of the ruby laser by a spark gap triggered by a part of the Nd laser beam[6]. Photographs were taken on Polaroid Type 47 film with a camera lens of 8 to 30 magnification. Selective filters were used to eliminate scattered light of the main laser beam. At the same time, photographs were taken of the main laser beam at the exit plane of the cell, in order to determine the total number of filaments produced in each experiment.

The main method used for detection and analysis of the filaments was to place the glass cell (selected for its negligible strain) containing liquid CS_2 between crossed polarizers, with polarization directions at 45° to that of the illuminating laser beam. Since filaments are known to be almost linearly polarized parallel to the polarization direction of the laser beam producing them[7], the birefringence $n_{\parallel} - n_{\perp}$, is given by $\lambda(I_{\perp}/I_{\parallel})^{\frac{1}{2}}/(\pi d)$ when the main laser beam is polarized perpendicular to the propagation direction of the illuminating light as in the present arrangement. In this expression, $I_{\parallel}$ is the power density of the illumination light of wavelength λ, $I_{\perp}$ is the power density of the perpendicularly polarized component produced by the filament and d is the filament diameter. While this method was chosen because it is one of the most sensitive for the detection of filaments we also used

Schlieren photography to measure the total amount of light scattered from the filaments. (An attempt to determine the sign of the refractive index change by using the phase-sensitive method[8] did not lead to a unique result.)

Typical filament traces excited by the 1.06 μ laser beam are shown in Fig. 1. These were produced in a cell 6 cm long and 2 cm thick, filled with liquid CS_2 at ~ 20°C. The main laser beam was focused beyond the exit end of the cell with a lens of relatively long focal length (~ 23 cm) compared to the cell length. The side-illuminating beam of 0.53 μ radiation covered the entire area shown in Fig. 1a and b.

The filament traces of Fig. 1a were photographed at 1 cm from the exit end of the sample cell. Approximately 15 traces can be seen; these were produced by a total of 30 filaments, as detected in photographs of the exit plane. (Usually, only about 1/5th of the filaments appeared to produce traces.) The lengths of the traces are 1 to 2 mm and their widths ~ 6 μ (as determined from photographs with larger magnification). Almost all filament traces were observed only in the region of coincidence of the main laser and illuminating beams, indicating that the filaments disappeared immediately after the light pulses had passed through the observation region. Thus, the lengths of the traces in Fig. 1a may be considered to give an upper limit to the filament duration times of approximately 5 to 10 picoseconds.

The production of filament traces shown in Fig. 1a finds a ready explanation in the birefringence caused by the optical Kerr effect. The intensity of individual filament traces ($\int I_\perp dt$) in

Fig. 1a is typically measured to be $\sim 10^{-4}$ of the time-integrated power density ($\int I_{\parallel} dt$) of the illumination light which enters the cell, although some traces are considerably more intense. Since each filament trace is presumed to be produced by only one of the 20 mode-locked pulses, whereas the measured intensity of the illumination light is the integrated intensity of all 20 pulses, the value $I_{\perp}/I_{\parallel}$ for individual filaments is $\sim 2\times10^{-3}$. For filament diameters d = 6μ, this value corresponds to a birefringence $n_{\parallel} - n_{\perp} = 1.2\times10^{-3}$. This value is much smaller than that (~ 0.2) reported by Brewer and Townes[9] for the special types of filaments observed by them but is in good agreement with the value estimated from the anti-Stokes rings in the stimulated Raman effect[10]. Furthermore, if we assume that the birefringence is due to the optical Kerr effect (which is based on the reorientational theory of molecules) the power density P within each filament, is calculated to be 60 GW/cm^2, from $n_{\parallel} - n_{\perp} = \left(\frac{\lambda}{\pi}\right) BE^2 = \left(\frac{4\lambda}{nc}\right) BP$ and using the known value for the Kerr constant B[11]. Therefore the energy in each filament is 1 to 2 ergs, in agreement with the reported value[3]. The true value for $n_{\parallel} - n_{\perp}$ is probably a little larger than 1.2×10^{-3}, because the actual duration time of filaments can be shorter than that calculated from the length of the traces in Fig. 1a (5 to 10 psec.), although it must be longer than the reorientational relaxation time for CS_2, ~ 2 psec[12]. Since $n_{\parallel} - n_{\perp}$ depends on the square root of $I_{\perp}/I_{\parallel}$, this correction does not exceed the factor $\sqrt{5}$. Therefore $n_{\parallel} - n_{\perp}$ is typically $2\pm1\times10^{-3}$, and does not exceed 10^{-2} even in the strongest traces.

In the above calculation of $I_{\perp}/I_{\parallel}$ we assumed that most of the

energy of the laser radiation was confined to the train of picosecond pulses with separation equal to the transit time of light in the laser cavity. Neither the oscilloscope traces nor the two-photon fluorescence technique[13] have sufficient resolution to confirm this since they cannot distinguish between a train of such sharp pulses or of sharp pulses superimposed on somewhat broader pulses. However, the same polarization technique as used above for the filaments was also used to determine the birefringence due to the whole laser beam and its power density. The birefringence produced by the laser beam at the entrance end of the sample cell is shown in Fig. 1b. The length of the broad white trace shows the temporal width of the picosecond pulse. From the density of this trace, the power density of the laser radiation was determined and the resulting estimate of the total energy in the picosecond pulses was in agreement, within a factor of two, with the energy measured directly with a calorimeter. Furthermore, no birefringence was detected when the coincidence between the two beams was shifted to a region outside that shown in Fig. 1b and we conclude that there was very little laser field outside of the picosecond pulses.

Other types of traces which were stationary in space and had longer duration times were also observed. They could be distinguished from the typical filaments of Fig. 1a by two characteristics: they appeared irrespective of the coincidence between the illuminating and main laser beams, and they were usually observed as dark lines, as seen in Fig. 1b. Since these dark lines were observed even in the pictures taken without polarizers, these traces persisted for a time comparable with the laser pulse. At relatively low excitation

power, the number of these traces was much smaller than the total number of the filaments as detected at the exit end. Most of them were observed close to the entrance end of the cell and rarely at the exit end. The mechanism of these traces is not clear; whatever the mechanism, the energy involved in this process seems to be larger than that required to produce the normal filaments (Fig. 1a). The relation of the two types of traces may be best explained as follows: Filaments with varying energy are formed in the first stage, but those with the larger energy lose much of their energy rapidly by other non-linear loss mechanisms leaving traces of the after-effect mainly in the entrance part of the cell. Only the filaments with relatively small energy of the leading edge of the filaments can travel to the exit end of the cell with small losses.

The traces of the filaments produced by the ruby laser, which were photographed close to the exit end of the cell showed similar characteristics and approximately the same birefringence as those in Fig. 1a. Their lengths were usually 1 to 2 mm but some traces were as long as 3 mm. The number of traces observed was much smaller than that of the filaments detected at the exit end of the cell (1/50 to 1/100), but this is not unreasonable, since only a small number is expected to coincide with the illumination light. The lengths of the traces indicate that the filament duration times are less than 15 psec. But it cannot be completely excluded that they are stationary traces in space, because the two laser beams (from ruby and Nd:glass) are independent and we cannot determine precisely the region of coincidence.

The present observations are limited by the relatively low sensitivity ($\Delta n \geq 10^{-3}$) and to filaments which are produced by particular types of lasers. However, this method is capable of detecting $\Delta n \simeq 10^{-4}$ in a 5-10μ filament by using a single spike of a mode-locked Nd laser and will be a useful tool to study various aspects of the optical trapping.

The authors would like to thank R.A. McLaren and A. Jares for experimental and technical assistance.

Figure Captions

Fig. 1. "Side pictures" of the mode-locked Nd laser beam and resulting filaments. The areas shown were illuminated by a collimated beam of polarized radiation (0.53 μ) and photographed through a crossed polarizer. The main laser beam producing the filaments travels from left to right. (a) 1 cm from the exit end of the cell showing filaments as sharp horizontal traces. (b) 1.5 cm from the entrance end of the cell with slightly higher power density than (a). One of the dark traces is seen to extend outside of the coincidence region (white broad trace). Circles and other irregular patterns are due to imperfections in the polarizers and to inhomogeneity of the illumination beam.

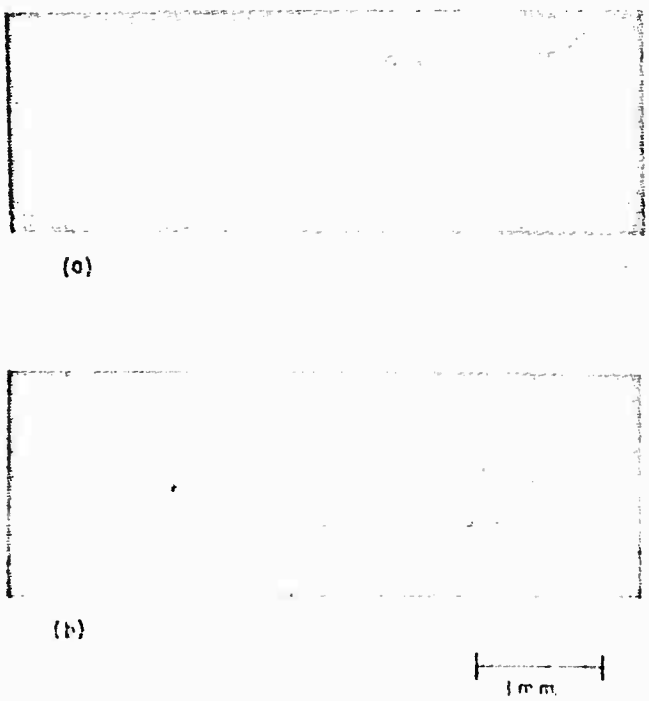

References

* This research is part of Project DEFENDER under the joint sponsorship of the Advanced Research Projects Agency, the Office of Naval Research, and the Department of Defense. Also supported in part by the National Research Council, Canada.

† Postdoctorate Fellow, University of Toronto. Present address: Division of Engineering and Applied Physics, Harvard University, Cambridge, Massachusetts, U.S.A.

1. R.Y. Chiao, M.A. Johnson, S. Krinsky, H.A. Smith, C.H. Townes and G. Garmire. "A new class of trapped light filaments" IEEE J. of Quantum Electronics, QE-2, 467-469 1966.

2. Present state of knowledge is summarized in R.G. Brewer, J.R. Lifsitz, G. Garmire, R.Y. Chiao and C.H. Townes, "Small-scale trapped filaments in intense laser beams" Phys. Rev. 166, 326-331 1968.

3. For filaments produced by the mode-locked Nd laser, R.G. Brewer and C.H. Lee, "Self-trapping with picosecond light pulses" Phys. Rev. Letters, 21 267-270 1968.

4. S. Saikan and H. Takuma, "Study of a self-trapped optical beam by high-speed holography" IEEE J. of Quantum Electronics, QE-4, 613-621 1968.

5. A.J. DeMaria, D.A. Stester and H. Heynau, "Self mode-locking of lasers with saturable absorbers" Appl. Phys. Letters 8 174-176 1966.

6. A.J. Alcock, C. DeMichelis and K. Hamal, "Subnanosecond Schlieren photography of laser-induced gas breakdown" Appl. Phys. Letters 12 148-150 1968.

7. D.H. Close, C.R. Giuliano, R.H. Hellwarth, L.D. Hess, F.J. McClung

and W.G. Wagner, "The self-focusing of light of different polarizations" IEEE J. of Quantum Electronics, QE-2, 553-557 1966.

8. For example, M. Born and E. Wolf, "Principles of Optics", Pergamon Press, New York pp. 425-426 1959.

9. R.G. Brewer and C.H. Townes, "Standing waves in self-trapped light filaments" Phys. Rev. Letters 18 196-200 1967.

10. C.A. Sacchi, C.H. Townes and J.R. Lifsitz, "Anti-Stokes generation in trapped filaments of light" Phys. Rev. 174 439-448 1968.

11. M.M. Paillette, "Mesures de l'effet Kerr induit par une onde lumineuse intense" Compt. Rendus. 262 264-266 1966.

12. S.L. Shapiro and H.P. Broida, "Light scattering from fluctuations in orientations of CS_2 in liquids" Phys. Rev. 154 129-138 1967.

13. J.A. Giordmaine, P.M. Rentzepis, S.L. Shapiro and K.W. Wecht, "Two-photon excitation of fluorescence by picosecond light pulses" Appl. Phys. Letters 11 216-218 1967.

High-Resolution Raman Spectroscopy of Gases with Laser Excitation*

W.R.L. Clements† and B. P. Stoicheff

The advent of the laser has paved the way for significant advances in high-resolution Raman spectroscopy (1). In earlier work with mercury lamp sources (1,2,3) the effective resolution was limited to ~ 0.3 cm^{-1} by the widths of the exciting lines. The intense 6328 Å line of presently available He-Ne lasers is almost one-tenth of this width, the maximum being approximately 0.05 cm^{-1}. To achieve an equally high resolution in Raman spectroscopy of gases, it is necessary to reduce both pressure and Doppler broadening and to use a dispersing instrument having a resolving power $\geq 3 \times 10^5$.

In this letter we describe a technique which has enabled us to take full advantage of the increased resolution provided by laser excitation. Spectra are obtained at pressures as low as the available laser intensity will permit. Observation is limited to small-angle scattering since the Doppler breadth associated with light scattering is a minimum in the forward direction (4). Motional narrowing (5) reduces this breadth further as shown by Cooper, May, Hara and Knaap (6) and Murray and Javan (7). Finally, the scattered radiation is analysed by a pressure-scanned Fabry-Perot interferometer (8) rather than by the traditional grating instruments.

Our experimental arrangement is shown in Fig. 1. Radiation at 6328 Å from a He-Ne laser 4 m long is used to excite the spectra; the total power is 400 mW in a line of full-width at half intensity ~ 0.025 cm^{-1}. The 6328 Å radiation is isolated with a 10 Å band-pass

filter and then focused in the scattering cell by a lens of 1 m focal length. The pyrex glass scattering cell is 1 m long and contains the sample gas at pressures up to 2 atm. This is followed by several narrow band-pass filters which block the laser light and transmit the scattered radiation under study. Radiation scattered at 2° is then collected by a conical lens and analysed with a pressure-scanned Fabry-Perot interferometer. For investigating rotational Raman lines with small frequency shifts it was found necessary to place a monochromator immediately in front of the F-P interferometer to be used in conjunction with, or instead of, the narrow band-pass filters. This not only helps to eliminate the laser light but also to isolate individual rotational lines. In addition, fluorescence originating in the interference filters, lenses and windows of the scattering cell (with maximum intensity at wavelengths longer than 6800 Å) was suppressed with the use of the monochromator.

Spectra of the S(1) rotational line of H_2 observed with both forward and 90° scattering are compared in Fig. 2. Both spectra were obtained at a gas pressure of 2 atm; the interferometer spectral free-range was 0.5 cm^{-1} and the effective resolution ~ 0.02 cm^{-1}. At 90° scattering, the full width at half maximum intensity of the line is 0.15 cm^{-1} and corresponds to the Doppler breadth at 20°C modified by motional narrowing. In the forward direction, the observed linewidth is reduced to 0.04 cm^{-1}. However, this value represents the total instrumental width (including the laser and interferometer linewidths); the true linewidth which is due, solely, to pressure broadening is 0.006 cm^{-1} at 2 atm (6).

Another example of the increased resolution achieved with this

technique is given in Fig. 3 which shows the narrow Q branch of the totally symmetric ν_1 band of CH_4. Its linewidth is ~ 0.3 cm^{-1}, which, as already noted was the limit of resolution in pre-laser work. The spectrum was obtained at 2 atm pressure, with the interferometer spectral free-range being 2.5 cm^{-1} and the total instrumental width ~ 0.07 cm^{-1}. Because of low intensity, a digital counter with a 500 sec counting interval was used and the observed spectrum is indicated by the solid circles in Fig. 3. It is possible to detect some structure within the narrow Q-branch observed with the present techniques. This structure is interpreted to be due to a small difference in rotational constants of the (0000) and (1000) levels with the spacing given by the usual expression $(B_1 - B_0) J (J + 1)$. Trial analyses were attempted with tentative rotational numbering of the observed peaks. The best numbering is that represented by the straight-line graph whose slope gives the value $B_1 - B_0 = - 0.0034$ cm^{-1} (Fig. 4). With this value of α_1, the relative positions of the rotational lines within the Q-branch were calculated and these are indicated in Fig. 3. Also, the relative intensities of the rotational lines were computed and assuming linewidths of 0.07 cm^{-1} a calculated spectrum was obtained. A comparison of this calculated spectrum with the observed spectrum shows satisfactory agreement.

The above preliminary investigations demonstrate that the laser is a potentially valuable excitation source for extremely high resolution Raman spectroscopy of gases.

REFERENCES

* This research is part of Project DEFENDER under the joint sponsorship of the Advanced Research Projects Agency, the U.S. Office of Naval Research, and the Department of Defense. Also supported by the National Research Council, Canada, and the University of Toronto.

+ Holder of Province of Ontario Scholarships 1968-1970.

1. A Weber, S.P.S. Porto, L. E. Cheesman and J. J. Barrett, J. Opt. Soc. Am. 57, 19 (1967).

2. M. A. Thomas and H. L. Welsh, Can. J. Phys. 38, 1291 (1960).

3. B. P. Stoicheff, Can. J. Phys. 32, 330 (1954); also Advances in Spectroscopy, Vol. I, H.W. Thompson, ed. (Interscience Pub. Inc., New York) pp. 91-174 (1959).

4. C. H. Townes, in Advances in Quantum Electronics, J. R. Singer, ed., (Columbia University Press, New York) pp. 3-11 (1961).

5. R. H. Dicke, Phys. Rev. 89, 472 (1953).

6. V. G. Cooper, A. D. May, E. H. Hara and H.P.P. Knaap, Can. J. Phys. 46, 2019 (1968).

7. J. Murray and A. Javan, J. Molecular Spectroscopy 29, 502 (1969).

8. P. Jacquinot, Rep. Progr. Phys. 23, 267 (1960); M. A. Biondi, Rev. Sci. Instr. 27, 36 (1956).

FIGURE CAPTIONS

1. Diagram of apparatus for high-resolution Raman spectroscopy of gases.

2. Profiles of the S(1) rotational line of H_2 gas at 2 atm pressure observed in forward and 90° scattering.

3. Q branch of the ν_1 band of CH_4 ($\Delta\nu$ = 2917 cm^{-1}) at 2 atm pressure. The solid circles o are experimental intensity points obtained with a digital counter using 500 sec intervals, and the dashed line - - - is the envelope of the computed spectrum.

4. Frequency separation of observed peaks from the J = 5 peak plotted against J(J + 1).

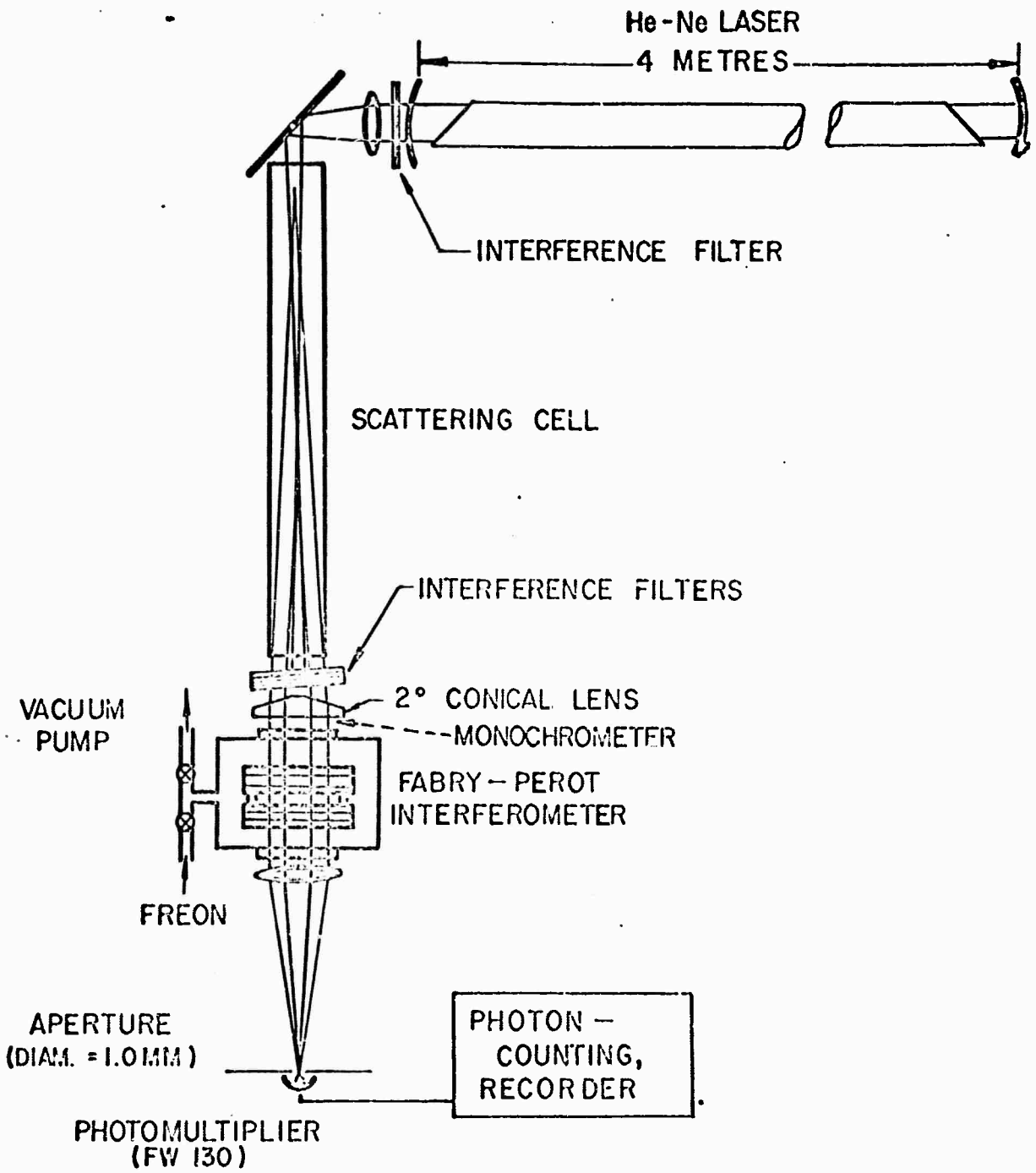
He-Ne LASER
4 METRES
INTERFERENCE FILTER
SCATTERING CELL
INTERFERENCE FILTERS
2° CONICAL LENS
MONOCHROMETER
VACUUM PUMP
FABRY – PEROT INTERFEROMETER
FREON
APERTURE (DIAM. = 1.0 MM)
PHOTON – COUNTING, RECORDER
PHOTOMULTIPLIER (FW 130)

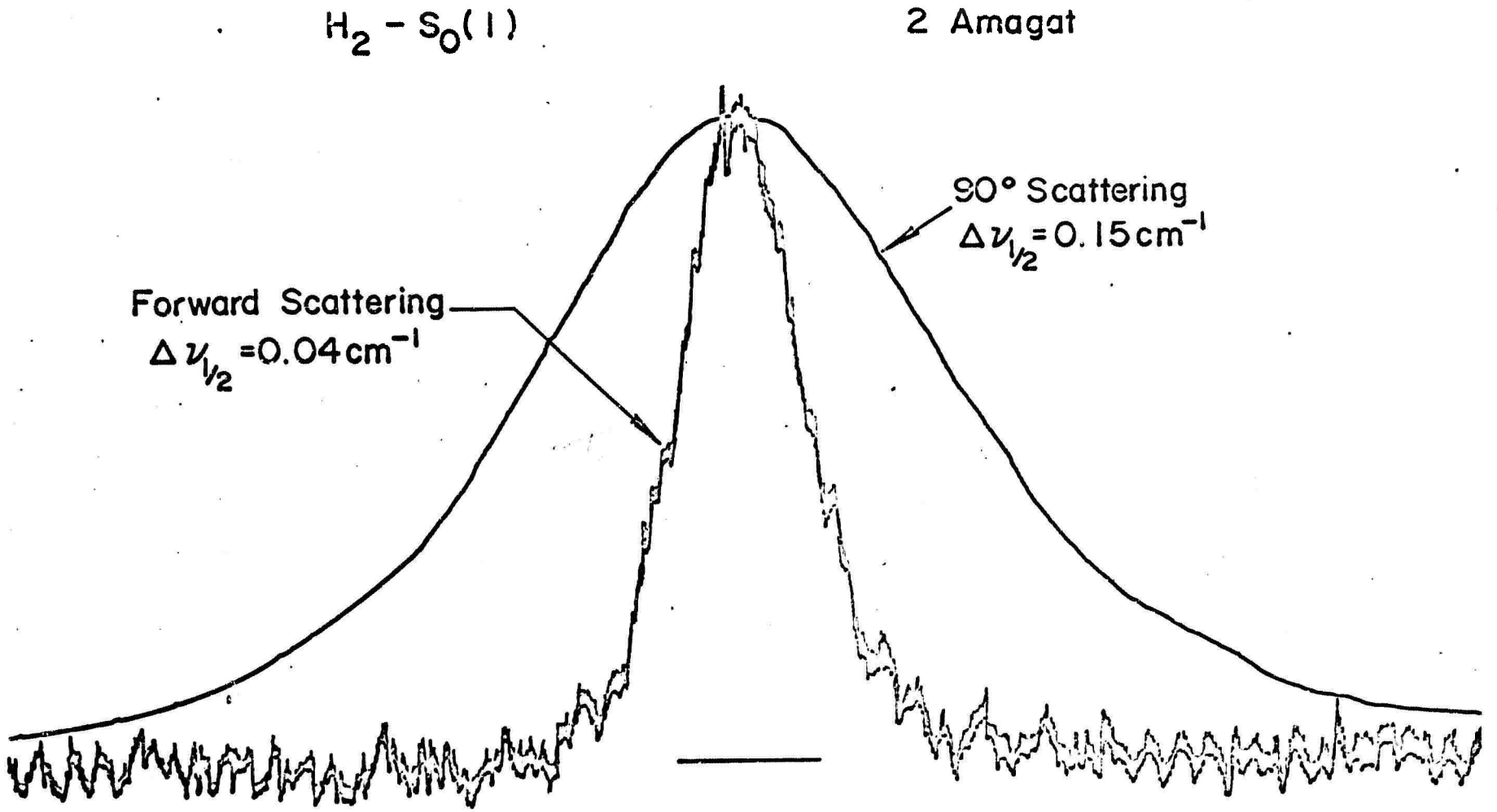
$H_2 - S_0(1)$
2 Amagat
90° Scattering
$\Delta\nu_{1/2} = 0.15\,cm^{-1}$
Forward Scattering
$\Delta\nu_{1/2} = 0.04\,cm^{-1}$

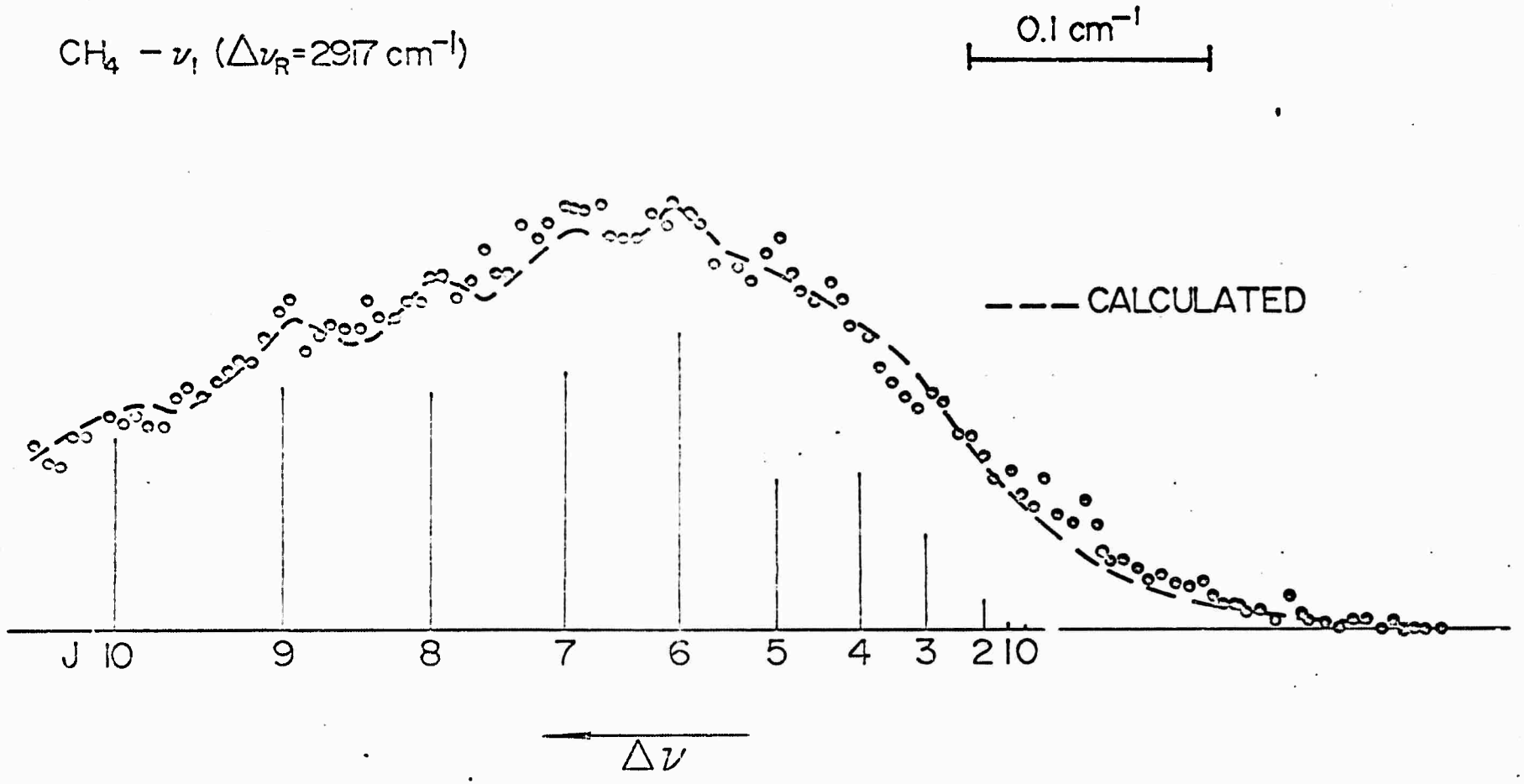
$CH_4 - \nu_1$ ($\Delta\nu_R$=2917 cm^{-1})
0.1 cm^{-1}
CALCULATED
J 10 9 8 7 6 5 4 3 2 1 0
$\Delta\nu$

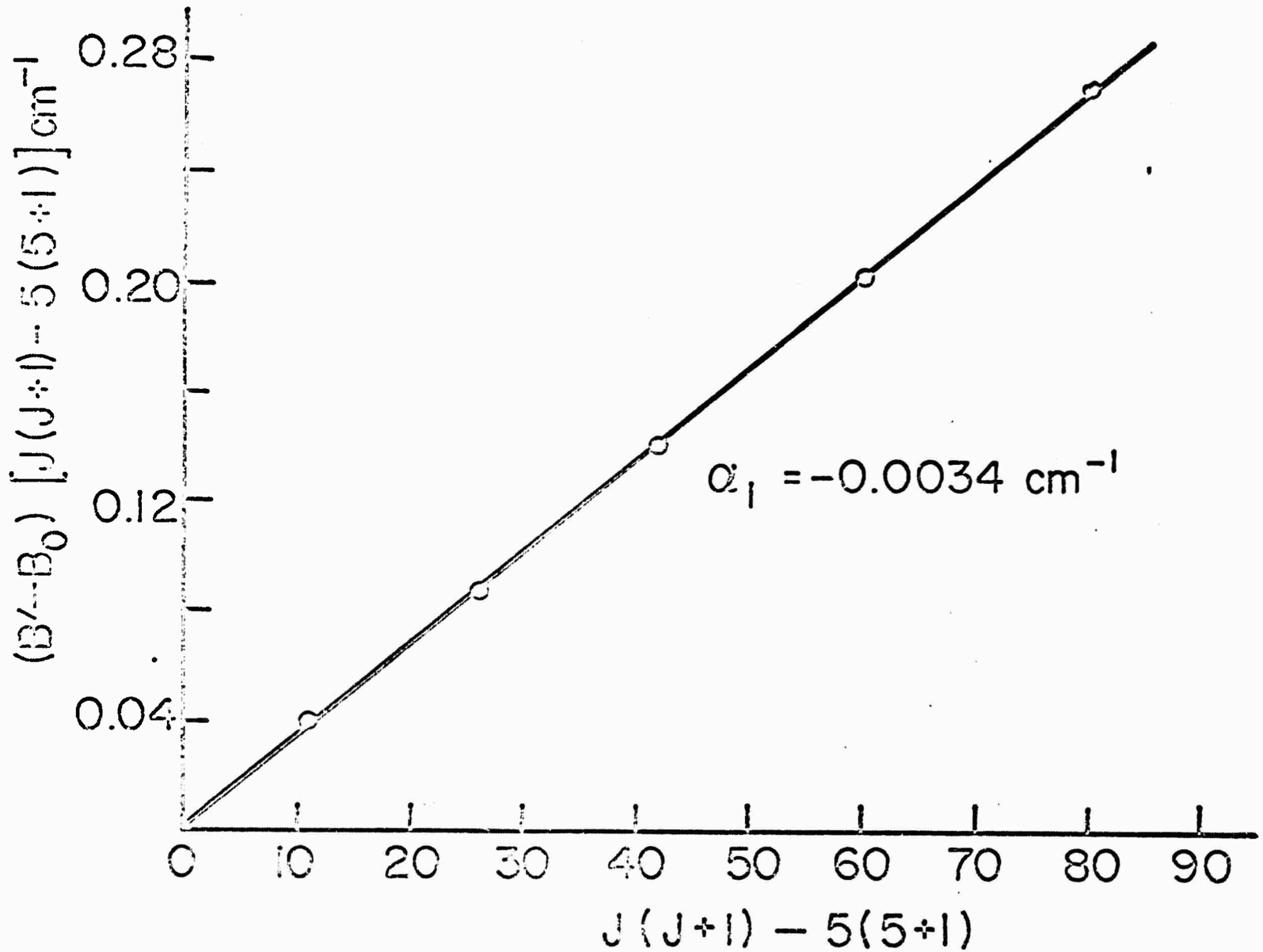
0.28
0.20
0.12
0.04
$(B'-B_0)\ [J(J+1)-5(5+1)]\,cm^{-1}$
$\alpha_1 = -0.0034\ cm^{-1}$
0
10
20
30
40
50
60
70
80
90
$J(J+1)-5(5+1)$

Stimulated Raman Emission in Diamond: Spectrum, Gain and Angular Distribution of Intensity†

A. F. McQuillan*, W.R.L. Clements‡ and B. P. Stoicheff

Department of Physics, University of Toronto

Toronto, Canada

Abstract

An experimental study of normal and stimulated Raman emission in diamond is presented including measurements of linewidth, intensity and angular distribution of radiation having a frequency shift of 1332.0 cm^{-1}. The diamond crystal formed a Raman resonator and excitation was by a giant-pulse ruby laser. The dependence of normal Stokes emission on laser intensity and the threshold for oscillation were investigated. A value for the Raman gain ($g = 6.9 \times 10^{-3}$ cm^{-1} per MW/cm^2) was calculated from the measured linewidth ($\Delta\nu = 2.04$ cm^{-1}) and cross-section for scattering, and found to be in good agreement with a value determined from the threshold for oscillation. The angular distributions of anti-Stokes and Stokes emission and absorption for parallel and convergent laser light are also in good agreement with theory: the emission cone angles are strongly dependent on the angle of convergence of the incident light and it is established that the preferred directions for emission are those making use of the most intense first-order Stokes radiation which is peaked in the forward direction within the Raman resonator.

Introduction

Numerous investigations[1] of the anomalous gain, angular distribution of intensity and spectral linewidths in stimulated Raman emission have been carried out with liquids, and none with gases. Corresponding studies with solids are rare. The first report of stimulated Raman emission in crystals (calcite, diamond and α-sulphur) was given in 1963 by Eckhardt, Bortfeld and Geller[2]. In 1964, Chiao and Stoicheff[3] made precise measurements of the anti-Stokes emission angles in calcite; Tannenwald[4] (1967) reported the observation of mode-pulling in a Raman resonator of crystalline quartz; and Bisson and Mayer[5] (1967-8) observed an anomalous gain in Raman resonators of calcite, the experimental gain being approximately ten times the calculated gain.

The present paper deals with the characteristics of the normal and stimulated Raman emission in diamond. Diamond is particularly well-suited for stimulated Raman experiments since the first-order Raman spectrum is known[6] to consist of a single sharp line of relatively high intensity. Therefore, the threshold for stimulated emission is expected to be low. The available diamond crystal was in the form of a plate with parallel surfaces, and because of the large refractive index of diamond, the plate served as a resonator: thus our experimental results have been strongly influenced by the properties of this resonator.

The main results of our investigations have been reported briefly on various occasions[7]. The linewidth and scattering cross-section were determined from the normal Raman spectrum. The intensity of normal Stokes emission was found to increase linearly with increasing laser intensity up to threshold for stimulated emission; this region was followed by a

sharp increase in intensity by a factor of $\sim 10^6$, and eventually by saturation and damage to the crystal. In a resonator, the onset of oscillation is governed by the condition $Fe^{(g-a)L} = 1$, where F is the feedback factor, g and a are the gain and loss constants and L is the crystal length. This condition was used to determine a value for the gain from the observed threshold for oscillation. A thorough study of the inhomogeneous intensity distribution of a laser and Stokes radiation in the resonator was also carried out in order to properly evaluate the gain constant. Good agreement was found between the value determined in this way and that calculated from the measured scattering cross-section and linewidth. Self-focusing was not apparent nor was stimulated Brillouin scattering detected at the power levels used in these experiments. The stimulated linewidth was observed to be an order of magnitude narrower than the normal linewidth, and on occasion two axial components of the Raman resonator were observed with evidence of mode-pulling and strong mode-interaction.

The angular distribution of intensity in the stimulated Raman emission was discussed in some of the first papers on the theory of the process[8-10]. From the momentum-matching condition based on a plane-wave model, maxima of anti-Stokes and Stokes emission (and the corresponding minima in first-order Stokes emission) are predicted according to the wave-vector relations

$$\vec{k}_o + \vec{k}_{n-1} = \vec{k}_{-1} + \vec{k}_n; \qquad \vec{k}_o + \vec{k}_{-1} = \vec{k}_{n-1} + \vec{k}_{-n} \tag{1}$$

Here $\vec{k}_o$, $\vec{k}_{-1}$, $\vec{k}_n$ and $\vec{k}_{-n}$ are, respectively, the laser, the first Stokes and the nth-order anti-Stokes and Stokes wave vectors. Such distribution of intensity in calcite was investigated by Chiao and Stoicheff[3] who found that agreement between the observed and calculated cone angles was within

the experimental error of a few percent, when an essentially parallel laser beam was incident on the calcite. In addition, they noted a significant increase in emission angles of anti-Stokes radiation as the focal length of the lens used to focus the laser beam was decreased. Shimoda[11] has discussed such an increase in cone angle with increase in angle of convergence of the laser beam; and Bloembergen and Shen[12] have considered multi-mode effects where two laser modes with a relative angle θ result in broadened anti-Stokes emission cones with an increase in apex half-angle of about $\theta/2$. We have made a detailed study of the angular dependence of anti-Stokes and Stokes radiation in diamond, and investigated in particular the changes in cone angles with different beam apertures and different beam convergence.

Experimental Procedure

The crystal of type II A diamond was in the form of a plate 2.18 mm thick and with flat, highly polished and almost parallel surfaces (wedge angle $\sim 10'$). Diamond has a refractive index of 2.4; thus the reflectivity at the air surfaces is 17% and the plate behaves as a Raman resonator. A Laue X-ray diffraction photograph established that the [111] axis of the crystal was approximately perpendicular to the polished faces of the diamond plate.

For measurement of the normal Raman linewidth, the spectrum was excited by λ 6328 radiation of a He-Ne laser and analysed with a Fabry-Perot interferometer, as described by Clements and Stoicheff[13]. In this experiment, the Fabry-Perot spacer was 0.869 ± 0.003 cm, mirror reflectivity was 99% and total laser plus instrumental width was 0.064 cm^{-1}.

The scattered light was observed at right angles to the incident beam.

Stimulated Raman emission was excited by λ 6940 radiation from a giant-pulse ruby laser. The radiation was plane polarized and was emitted in a single pulse of ~ 30 nsec duration and in a single (or nearly single) axial mode. Good reproducibility in the laser pulse was obtained by firing the laser at constant power near threshold at regular intervals with the ruby at a constant temperature (-10°C).

The experimental arrangement for photographing the stimulated Raman spectrum and for measuring its intensity is shown in Fig. 1. Laser radiation was incident on an aperture of 3.6 mm diameter and its intensity was measured by a 931A (RCA) phototube. A lens of 18 cm focal length was used to focus the laser beam 2 cm beyond the diamond crystal. Radiation scattered in the forward direction was focused on the slit of the grating spectrograph. Photographs of the Raman spectrum were obtained with a 1 cm^{-1} slit width, and a reciprocal linear dispersion of 20 cm^{-1}/mm. Some photographs were also obtained at much higher resolution, with the spectrograph replaced by a Fabry-Perot interferometer and a 1 metre camera lens.

For measuring the intensity of first-order Stokes radiation, the method used was that described in a recent study in this laboratory[14] of intensity measurements in liquid O_2 and F_2. The laser radiation was varied by inserting neutral density filters in the beam at the entrance aperture. Radiation scattered in a cone of 3.9×10^{-3} sr was collected through an aperture and focused on the slit of the spectrometer. A 7102 (RCA) phototube was used to detect the Stokes radiation and the Stokes and laser signals were displayed on a dual beam oscilloscope (Tektronix 555). The pulse heights gave effective measurements of the Stokes and laser intensities. The transmission characteristics of the spectrometer and

attenuating filters as well as the sensitivity of the phototubes were determined and the complete arrangement was calibrated by measurements with benzene, all as described in the earlier work[14]. The measured Raman intensity is estimated to be accurate to ± 30%.

For observation of the angular distribution of intensity, the same arrangement as Fig. 1 was used but with the optical elements after the diamond crystal replaced by a camera. Appropriate filters were placed in front of the camera to isolate the various Stokes and anti-Stokes frequency components.

The Spectrum

The normal Raman spectrum of the diamond crystal consists of a single line at a frequency shift of 1332 cm^{-1}. This line was found to have a Lorentzian lineshape with full width at half intensity maximum measured to be 2.04 ± 0.04 cm^{-1}, at room temperature. Measurements of the linewidths exhibited by two other diamond crystals (also type II) gave similar values, namely 2.09 ± 0.04 and 2.22 ± 0.04 cm^{-1}.

Photographs of the stimulated Raman spectrum of diamond revealed four sharp lines, two being the first- and second-order Stokes lines and two the corresponding anti-Stokes lines. Their frequency shifts from the exciting line were measured to be 1331.8 ± 2 cm^{-1} and double this value, corresponding to the fundamental and exact multiple of the C-C vibrational frequency. Examination of the first-order Stokes line at high resolution with a Fabry-Perot interferometer (Fig. 2) showed that its width was very narrow, with variation of 0.1 to 0.2 cm^{-1}, from shot to shot of the laser. This spectral width is at least one-tenth that of the normal Raman line, yet considerably larger than that of the laser exciting line.

In approximately ten percent of these photographs the stimulated Stokes line was split into two components separated by 0.35 ± 0.15 cm^{-1} (Fig. 2) while the laser exciting line itself remained single and sharp. Further study of the spectrum, with the emission region of the crystal magnified 20 X (Fig. 3) and 100 X revealed the presence of many regions of oscillation each approximately 50 μ wide and 100 to 150 μ long. Their size was governed partly by the multiple beam interference fringes with spacing $\lambda/(2n\delta) \approx 55$ μ, corresponding to the 10' tilt δ between the polished faces of the crystal, and perhaps also due to imperfect surfaces or to the existence of many crystallites. (Spectra observed with a tilted Fabry-Perot interferometer and 100 X magnification indicated that these regions sometimes oscillated independently of one another, some in a single mode, others in two axial modes, with the magnitude of the splitting and the intensity ratio of the two modes varying from region to region.)

The average mode separation in our diamond resonator is $1/(2nL) \approx 1$ cm^{-1}, which is approximately half the normal Raman linewidth. Under these conditions there should be strong mode-pulling, as observed by Tannenwald[4] in Raman resonators of quartz. Mode-pulling would be expected to decrease the mode separation by the factor $(1 - \Delta\nu_c/\Delta\nu_a)$ where $\Delta\nu_a$ is the normal Raman linewidth and $\Delta\nu_c$ is the cavity linewidth defined in the usual way as $\Delta\nu_c = \alpha'/(2\pi nL)$, with α' the fractional power loss, $(1 - \mathcal{R})$, at the cavity surfaces. For ideal surfaces $\Delta\nu_c \sim 0.3$ cm^{-1}, however as shown by the width of the fringes in Fig. 3, the value for our crystal is approximately twice this value, that is $\Delta\nu_c \approx 0.6$ cm^{-1}. This would lead to a decrease of the mode separation from a value of ~ 1 cm^{-1} to ~ 0.7 cm^{-1}, still somewhat larger than the observed separations in the

range 0.2 to 0.5 cm^{-1}. Further decrease could arise from an absorption loss[4] related to focusing geometry or from strong electric-field interaction effects as observed in gas lasers[15] when the cavity mode-spacing and the normal (spontaneous) linewidth are almost the same, as in the present experiment.

Intensity of Stokes Radiation and Raman Gain

The observed intensity of first-order Stokes radiation and its dependence on incident laser intensity is shown in the graph of Fig. 4. At low laser power, normal Raman emission was observed, and this increased linearly with increasing laser power. The threshold for oscillation occurred at a laser power of 1.05 MW and Stokes intensity increased sharply by a factor of about 10^6 for an increase in laser power to 1.5 MW. At higher laser powers, saturation set in and further increase resulted in damage to the crystal.

The region of normal Raman emission is shown in more detail in Fig. 5, which clearly illustrates the linear increase of Stokes power with increasing laser power. The measured slope of this graph was used to obtain a value for the total Raman scattering efficiency S, which is defined as the ratio of the number of scattered photons at frequency ω_s (produced per unit time per unit cross-sectional area of crystal in a solid angle Ω about the direction of observation) to the number of incident photons of frequency ω_0 crossing unit area in unit time. The experimental value of S is given by $(P_r/P_0)(1/L\Omega)$, where P_r is the Raman power for the whole Raman line scattered into the solid angle Ω, P_0 is the corresponding laser power, and L is the path length. A value of

$S = 2.7 \times 10^{-7}$ cm^{-1} sr^{-1} was obtained, having an estimated accuracy of $\pm$ 30%. How S is related to $d\alpha/dx$, the rate of change of electronic polarizability per unit cell with relative displacement of the atoms, and according to Smith[16] and Loudon[17] is given by

$$S = \frac{3\hbar N^2 \omega_s^4}{2\pi c^4 \rho \omega_o} \left|\frac{d\alpha}{dx}\right|^2 (n_o + 1)$$

Here $\omega_s = \omega_o - \omega_r$ is the Stokes angular frequency, ω_o is the laser frequency and $\omega_r = 1332$ cm^{-1}; N is the number of unit cells per unit volume, n_o is the Bose population factor (with $n_o + 1 \sim 1$ at room temperature) and ρ is the crystal density. From the above value of S we obtain $d\alpha/dx = 4.6 \times 10^{-16}$ cm^2 per unit cell, for laser radiation propagating along the [111] axis of the crystal. This value is in good agreement with the value 4.0×10^{-16} cm^2 obtained by Anastassakis, Ivasa and Burstein[18] from electric-field-induced infrared absorption in diamond.

The Raman gain per unit length of active medium is defined by

$$g = \frac{16\pi^2 c^2 S_{//} I_o}{\hbar n^2 \omega_s^3 \Delta\nu}$$

Here, $S_{//}$ is the scattering efficiency of radiation polarized in the same plane as the incident plane polarized laser radiation, and equals $S/(1 + d)$, where d ($= I_\perp / I_{//}$) is the depolarization ratio; $\Delta\nu$ (cm^{-1}) is the full width at half intensity of the normal Raman line, n is the refractive index of the medium, I_o is the incident laser intensity, and the remaining symbols have their usual meanings. With the above experimental values of $S = 2.7 \times 10^{-7}$ cm^{-1} sr^{-1}, d = 0.60 and $\Delta\nu = 2.04$ cm^{-1} the Raman gain in diamond is calculated to be $g = 6.9 \times 10^{-3} I_o$ cm^{-1} with I_o in MW/cm^2.

This value for the Raman gain determined entirely from the characteristics of the normal Raman spectrum can now be tested with the observed

threshold for oscillation. As already noted in the Introduction, the condition for oscillation threshold is $F \exp[(g-\alpha)L] = 1$. The feedback factor $F \equiv$ reflectivity $= 0.17$; the loss constant α was considered to be negligible (since the observed scattering and absorption losses at low intensities with the ruby laser were small) and diffraction losses for such a small path length are also expected to be small relative to g. Thus the threshold condition reduces to $e^{gL} = 5.9 = e^{1.8}$, or $gL = 1.8$; that is, at threshold $g = 8.2$ cm^{-1}. From the above values, $g = 8.2 = 6.9 \times 10^{-3} I_o$, the laser intensity at threshold would be expected to be $I_o \approx 1200$ MW/cm^2.

According to Fig. 4 the laser power at threshold as measured by PM-1 is 1.05 MW. The spatial intensity distribution of the laser and Stokes radiation was investigated by taking near-field photographs (at magnification of 20X) of th illuminated area of the crystal. The laser beam cross-sectional area at the crystal was measured to be 0.37 mm^2: however, the area of maximum intensity was determined to be 0.2 mm^2 (by interposing neutral density filters in the beam) and this area is shown in Fig. 3. Accordingly the laser intensity incident on the crystal at threshold is $1.05/0.002 \approx 530$ MW/cm^2. The intensity within the crystal, however, is modified because the crystal forms a resonator. This behaviour is evident in the near-field photographs (Fig. 3) of both the laser and Stokes radiation, which show interference fringes with spacing ≈ 55 μ, caused by the slight wedge between the polished faces of the crystal. For such multiple-beam interference, the fringe maxima have intensity equal to that of the incident light, I_o, and the minima have intensity $[(1-R)/(1+R)]^2 \approx 0.5 I_o$ for diamond with 17% reflectivity. Also, the finesse ≈ 1.5, that is, the fringe width is somewhat less than the fringe spacing (Fig. 3). At threshold, only the intensity maxima, comprising at most half the laser

beam area at the crystal, will be effective in generating stimulated Stokes radiation. Therefore, according to this analysis, the laser intensity at threshold is at least 530/0.5 or ~ 1100 MW/cm^2. This apparently excellent agreement with the expected value of ~ 1200 MW/cm^2 is, no doubt, fortuitous; the experimental values of S and S// have accuracies of ~ 30% and intensity peaks in the fringe maxima of the laser radiation are indicative of spatial inhomogeneity in the laser beam. In spite of these uncertainties, the observed low oscillation threshold in diamond appears to be within a factor of about two of the value calculated from the Raman gain $g = 6.9 \times 10^{-3} I_0$.

Angular Distribution of Intensity

Owing to the thinness of the diamond crystal available, some focusing of the incident laser light was necessary to observe stimulated emission. With the use of a long focal length lens (f ≈ 30 cm) and almost parallel exciting radiation, the emission cones of the first three orders of anti-Stokes and of the second-order Stokes radiation were observed along with the corresponding intensity minima in the diffuse first-order Stokes emission. The measured values of the cone angles are given in Table I and, for comparison, the values calculated from Eq. 1 are included. In these calculations tabulated values of the refractive index over the wavelength range 4861 Å to 7593 Å were used[19]. It is seen that the agreement is very good for all of the emission angles observed, although not as good for the Stokes minima which were difficult to measure. We conclude that just as for calcite, the theory of the plane-wave phase matching conditions is applicable to diamond.

No intensity dependent change in cone angles was observed at incident laser power densities from threshold up to 2.5 times threshold. Although an intensity dependence in the direction of maximum anti-Stokes intensity has been predicted by Bloembergen and Shen[9], the theoretical change in cone half-angle over this range is $\sim 2 \times 10^{-3}$ radians. The necessity of using strongly convergent incident light (convergence angle 0.023 rad.) to cover this intensity range, and the broadness of the anti-Stokes rings, make comparison with theory inconclusive.

The cone angles are very sensitively dependent on the angle of convergence of the incident laser beam even at threshold. A series of experiments was carried out in which the laser radiation was focused by lenses of different focal lengths and then incident on the diamond crystal. Focal lengths of 2.7, 3.3, 5.2, 9.8, 17.4, 26.0, 31.0 and 50.0 cm were used and, as before, photographs of the first- and second-order anti-Stokes and of the second-order Stokes "rings" were obtained. The corresponding angles are plotted against the reciprocal of the focal length in Fig. 6. A linear relation is evident for the anti-Stokes cone angles with the angles increasing as the focal length becomes shorter. Thus $\theta_{AS} \propto 1/f$. However, the second-order Stokes cone angles show a completely different dependence on focal length. The angle decreases sharply with shorter focal lengths and appears to reach a limiting value of about 0.065 radians.

In another series of experiments the dependence of the cone angles on the aperture of the incident radiation was investigated. A lens with f = 5.15 cm was used to focus the laser beam. Apertures of 1.0, 1.6, 1.9, 2.4, 2.8, and 3.6 mm diameter were placed in turn at the centre of the lens and photographs of the rings were obtained. The results are shown in a graph of anti-Stokes cone angle versus aperture diameter in Fig. 7.

The results clearly indicate a linear relation $\theta_{AS} \propto i$.

These two series of experiments establish the result that the cone angles of anti-Stokes emission depend on the angle of convergence of the incident exciting radiation. More precisely, the change in angle is given by $\Delta\theta_{AS} = K(a/f)$ where K is a constant, a the aperture radius and f the focal length. The first anti-Stokes cone angles are therefore given by $\theta_{AS} = 0.053 + K(a/f)$ where a/f defines the cone angle of the periphery of the converging laser beam. This result implies that the wave vector relations of Eq. 1 are rotated by the angle K(a/f) as shown in Fig. 8. The numerical value of K is 0.9 ± 0.2.

According to the theory of the stimulated Raman process, anti-Stokes radiation is generated by terms of the form $\chi_a E_0^2 E_s$ where χ_a is the susceptibility at $\omega_0 + \omega_r$ and E_0 and E_s are the electric fields at ω_0 and $\omega_0 - \omega_r$. The generation of anti-Stokes radiation is coupled to Stokes radiation and the direction of maximum intensity will depend on the direction of maximum intensity of laser and Stokes radiation. Once these directions have been established, the anti-Stokes cone angles can be determined from the momentum matching condition.

All of our observations can be explained in this way provided that first-order Stokes radiation is predominantly in the forward direction. This condition was satisfied in our experiment; the diamond was set with polished faces approximately perpendicular to the beam axis so that when either parallel or convergent light was incident on the crystal, Stokes radiation along the beam axis was favoured. Also, spurious scattering of Stokes radiation within the crystal or at its surfaces ensured the presence of Stokes radiation at half-angles of $\sim 6^\circ$ to the forward direction.

When laser and Stokes radiation interact to produce anti-Stokes

emission, that direction will be preferred which makes use of intense Stokes radiation closest to the resonator axis. With a converging incident beam it is possible to couple to Stokes closer to the axis and still satisfy the phase matching conditions. This results in an increase in anti-Stokes emission angle with a/f, up to the extreme case of anti-Stokes emission at 0.053 + 0.064 radians (see Table I) and Stokes radiation on axis. Experiments were performed to observe the behaviour of the anti-Stokes emission at values of a/f greater than 0.064 (Fig. 9). Convergence angles of 0.091 and 0.112 were used. In both cases the system was somewhat "confused" giving very broad emissions. With a convergence angle of 0.112 radians, two maxima were present in the anti-Stokes emission. The more intense one corresponded to a cone angle of about 0.11 rad. (with Stokes along the axis), and the weaker ring corresponded to an angle of 0.15 rad. (with Stokes slightly off axis and laser radiation at the periphery of the beam).

The dependence of the second-order Stokes emission angle on convergence of the laser beam further illustrates the preference of the higher-order Raman emissions to couple to Stokes close to the axis. From the wave vector diagram in Fig. 8, it is seen that, with increasing angle of the laser radiation, first-order Stokes radiation closer to the axis is effective in producing second-order Stokes emission. However, the emission angle decreases with increasing angle of convergence of laser radiation. It appears to reach a limiting value of about 0.07 rad ($\sim 0.116 - 0.043$) with Stokes radiation on axis. This explains the observed behaviour shown in Fig. 6.

It is also evident from the above explanation of the importance of beam convergence, that when a cylindrical lens (or a spherical lens with

a long slit as aperture) is used to focus the laser beam, the "ring" pattern will be replaced by "elliptical" patterns, the minor axis being determined by the cylinder axis (or width of slit). Moreover maxima of intensity will occur at the extremities of the major axis produced by converging light, since the gain would be largest for Stokes radiation closest to the beam axis. "Elliptical" patterns exhibiting these features have been observed with calcite and with Class I radiation in liquids[20]. An example of such a pattern obtained by focusing with a cylindrical lens in diamond is shown in Fig. 10.

Conclusion

The present investigation has combined the study of the stimulated Raman effect in a solid with the behaviour of a Raman oscillator. As in an earlier study with liquid O_2 and N_2, the stimulated Raman effect in diamond is simplified by the absence of self-focusing and stimulated Brillouin scattering. The experimental results are consistent with theory. This study of the angular properties of stimulated emission confirms the earlier results obtained with calcite, and extends our knowledge of the production of Class I radiation in solids.

Also, in this study, the value of the Raman gain determined from the measured cross-section and linewidth of normal Raman scattering gives an oscillation threshold which is in reasonable agreement with the observed value.

We are grateful to Dr. J. M. Orun for assistance with the intensity measurements and to Drs. R. H. Stolen and F. Shimizu for valuable discussions.

References

† This research is part of Project DEFENDER under the joint sponsorship of the Advanced Research Projects Agency, the U.S. Office of Naval Research and the Department of Defense. Also supported by the National Research Council, of Canada and the University of Toronto.

* Holder of Province of Ontario Government Scholarships 1965-68; Present address, Department of Physics, York University, Toronto, Canada.

* Holder of Province of Ontario Government Scholarships 1968-69.

1 N. Bloembergen, Am. J. Phys. 35, 989 (1967).

2 G. Eckhardt, D. P. Bortfeld and M. Geller, Appl. Phys. Letters 3, 137 (1963).

3 R. Y. Chiao and B. P. Stoicheff, Phys. Rev. Letters 12, 290 (1964).

4 P. E. Tannenwald, J. Appl. Phys. 38, 4788 (1967).

5 G. Bisson and G. Mayer, C.R. Acad. Sci. Paris 265, 397 (1967); J. de Phys. 29, 97 (1968).

6 R. S. Krishnan, Proc. Indian Acad. Sci. A24, 45 (1946).

7 A. K. McQuillan and B. P. Stoicheff, Bull. Am. Phys. Soc. 12, 60 (1967); IEEE J. Quant. Electronics QE-4, 381 (1968).

8 E. Garmire, E. Pandercse and C. H. Townes, Phys. Rev. Letters, 11, 160 (1963).

9 N. Bloembergen and Y. R. Shen, Phys. Rev. Letters 12, 504 (1964); Phys. Rev. 137A, 1787 (1965).

10 P. D. Maker and R. W. Terhune, Phys. Rev. 137A, 801 (1965).

11 K. Shimoda, J. Appl. Phys. Japan 5, 86 (1966).

12 N. Bloembergen and Y. R. Shen, Phys. Rev. Letters 13, 720 (1964).

13 W.R.L. Clements and B. P. Stoicheff, Appl. Phys. Letters 12, 246 (1968).

14 J. B. Grun, A. K. McQuillan and B. P. Stoicheff, Phys. Rev. 180, 61 (1969).

15 W. J. Witteman, Phys. Rev. 143, 316 (1966).

16 H.M.J. Smith, Phil. Trans. Roy. Soc. A241, 105 (1948).

17 R. Loudon, Advances in Phys. 13, 423 (1964).

18 E. Anastassakis, S. Iwasa and E. Burstein, Phys. Rev. Letters 17, 1051 (1966).

19 Landolt-Bornstein, Physik.-Chem. Tabellen, Vol. II (Julius Springer, Berlin, 1923) p. 918.

20 E. Garmire, Phys. Letters 17, 251 (1965); in Physics of Quantum Electronics edited by P. L. Kelley, B. Lax and P. E. Tannenwald (McGraw-Hill Book Company, Inc., New York 1966) pp. 167-179.

Table I

Comparison of theoretical and experimental values of the emission and absorption angles (in radians) observed in diamond

Frequency	Emission Angles		Absorption Angles	
	Expt.	Theory	Expt.	Theory
$\omega_o - 2\omega_r$	0.116	0.119	(0.048)[a]	0.043
$\omega_o + \omega_r$	.053	.053	.060	.064
$\omega_o - 2\omega_r$	.103	.104	(.079)	.071
$\omega_o + 3\omega_r$	.158	.152	----	.079

[a]Values in brackets are measurements of weak and broad absorption rings.

Figure Captions

Fig. 1 Schematic diagram of apparatus for intensity measurements. Explanation of symbols: F - attenuating filter, D - diaphragm, L - lens, S - spectrometer, PM - photomultiplier detector.

Fig. 3 Near-field patterns of (a) laser radiation in the diamond crystal below threshold for stimulated Raman emission, and (b) stimulated Stokes radiation.

Fig. 2 Fabry-Perot interferogram of Stokes radiation showing two oscillating modes separated by $\sim 0.3\ cm^{-1}$. The inter-order spacing is $\sim 3\ cm^{-1}$.

Fig. 4 Experimental curve of Raman Stokes power versus incident laser power.

Fig. 5 Experimental curve of normal Raman scattering power versus incident laser power. The arrow indicates the onset of oscillation.

Fig. 6 Graphs of emission angles observed for first- and second-order anti-Stokes (AS_1 and AS_2) and for second-order Stokes (S_2) radiation as a function of inverse focal lengths of lenses used to focus laser radiation.

Fig. 7 Graph of first-order anti-Stokes emission angle as a function of limiting aperture diameter of converging laser beam.

Fig. 8 Diagrams of changes in (a) first-order anti-Stokes emission angle, and (b) second-order Stokes emission angle, with change in direction of first-order Stokes wave vector k_1.

Fig. 9 Graph of first-order anti-Stokes emission angle as a function of convergence angle of incident laser beam.

Fig. 10 Elliptical anti-Stokes radiation pattern obtained by focusing laser beam with a cylindrical lens.

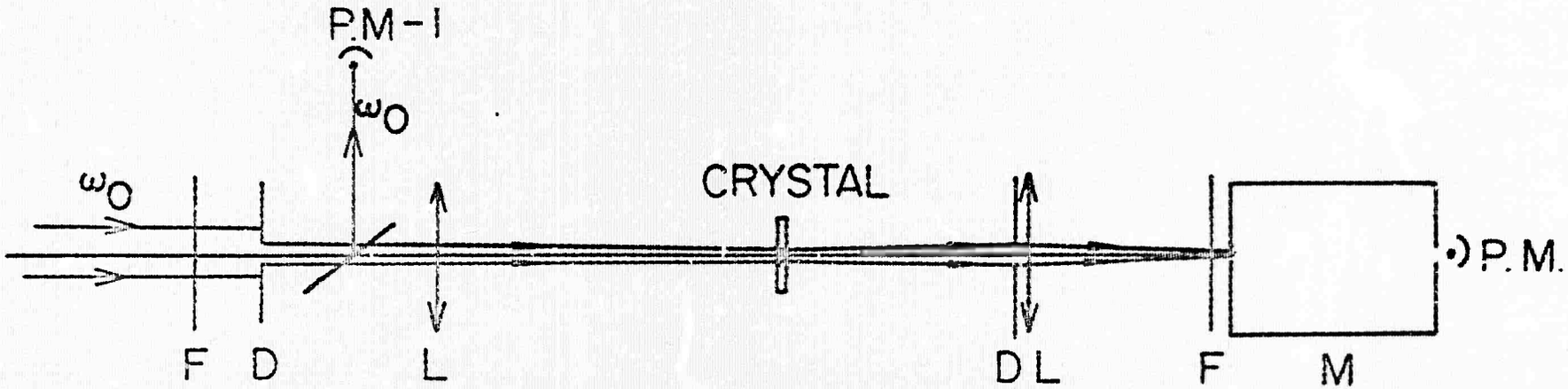

FIG. 1.

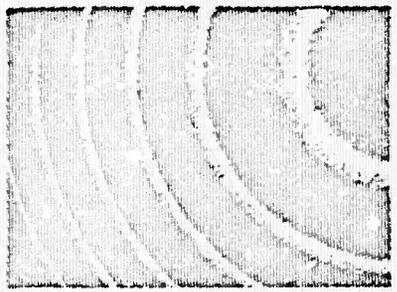

FIG. 2.

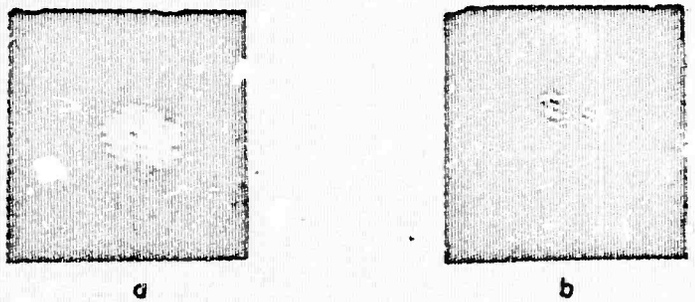

FIG. 3

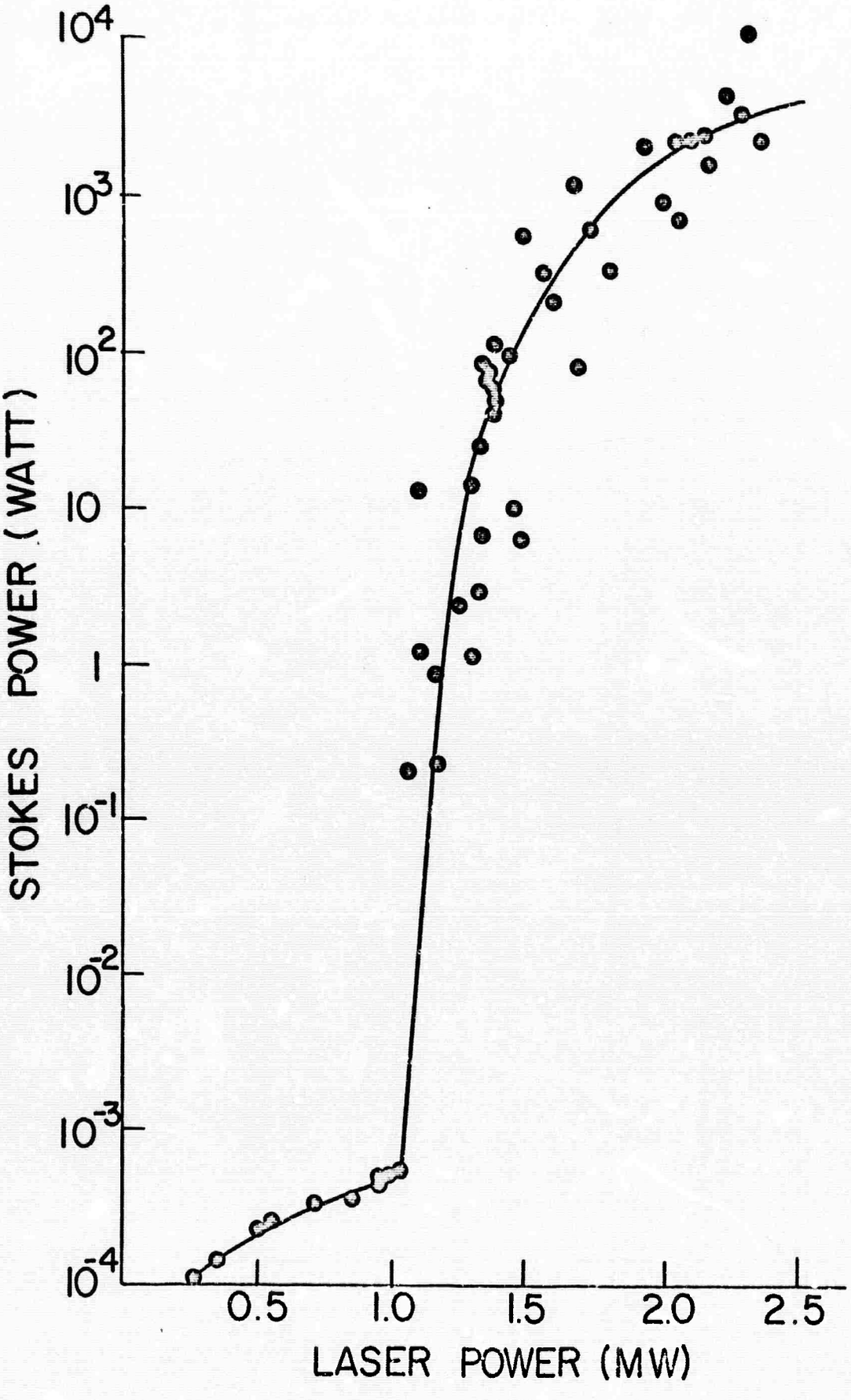
STOKES POWER (WATT)
10^4
10^3
10^2
10
1
10^{-1}
10^{-2}
10^{-3}
10^{-4}
0.5
1.0
1.5
2.0
2.5
LASER POWER (MW)

FIG. 4.

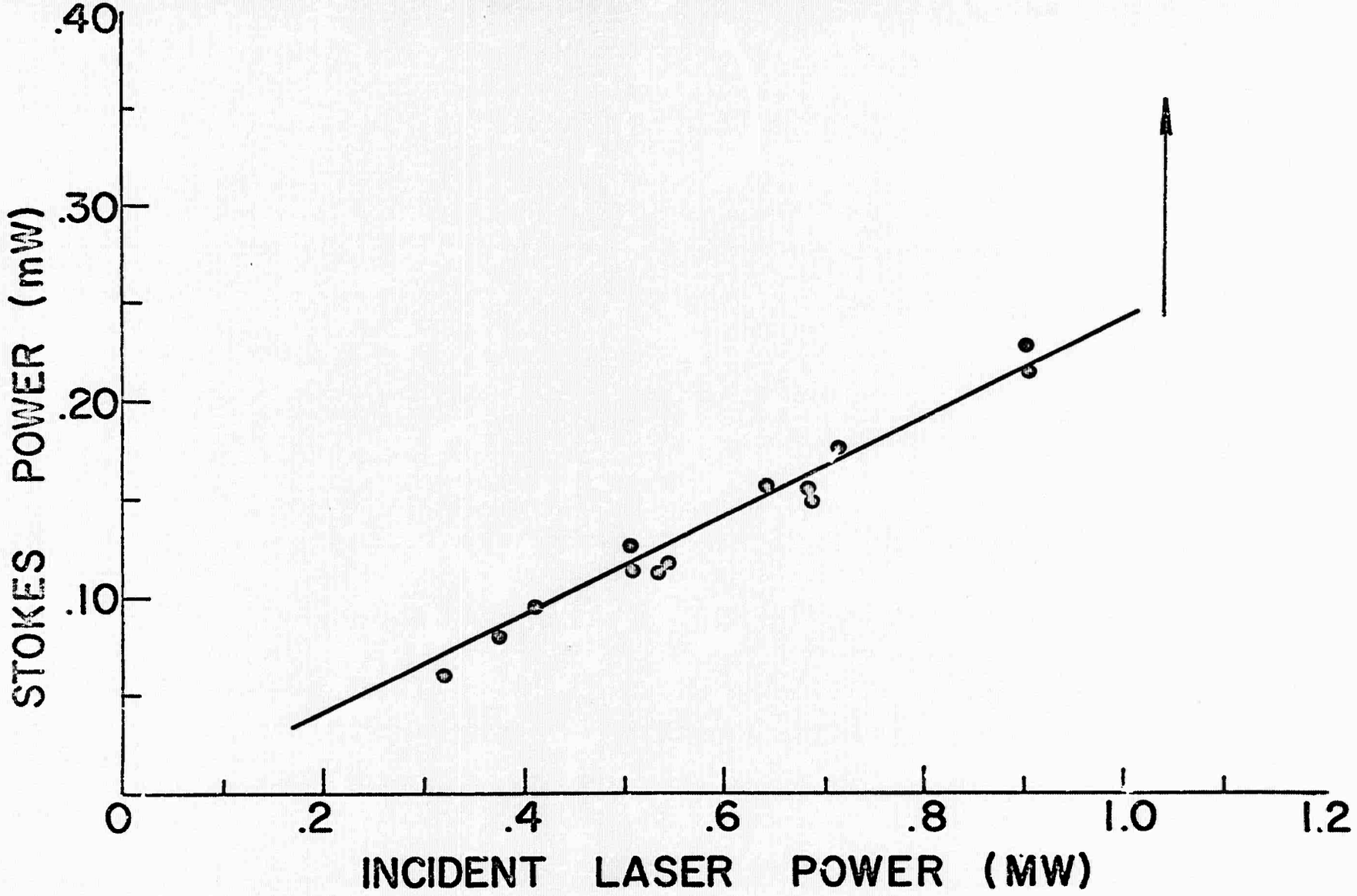
.40
.30
.20
.10
STOKES POWER (mW)
0
.2
.4
.6
.8
1.0
1.2
INCIDENT LASER POWER (MW)

FIG. 5

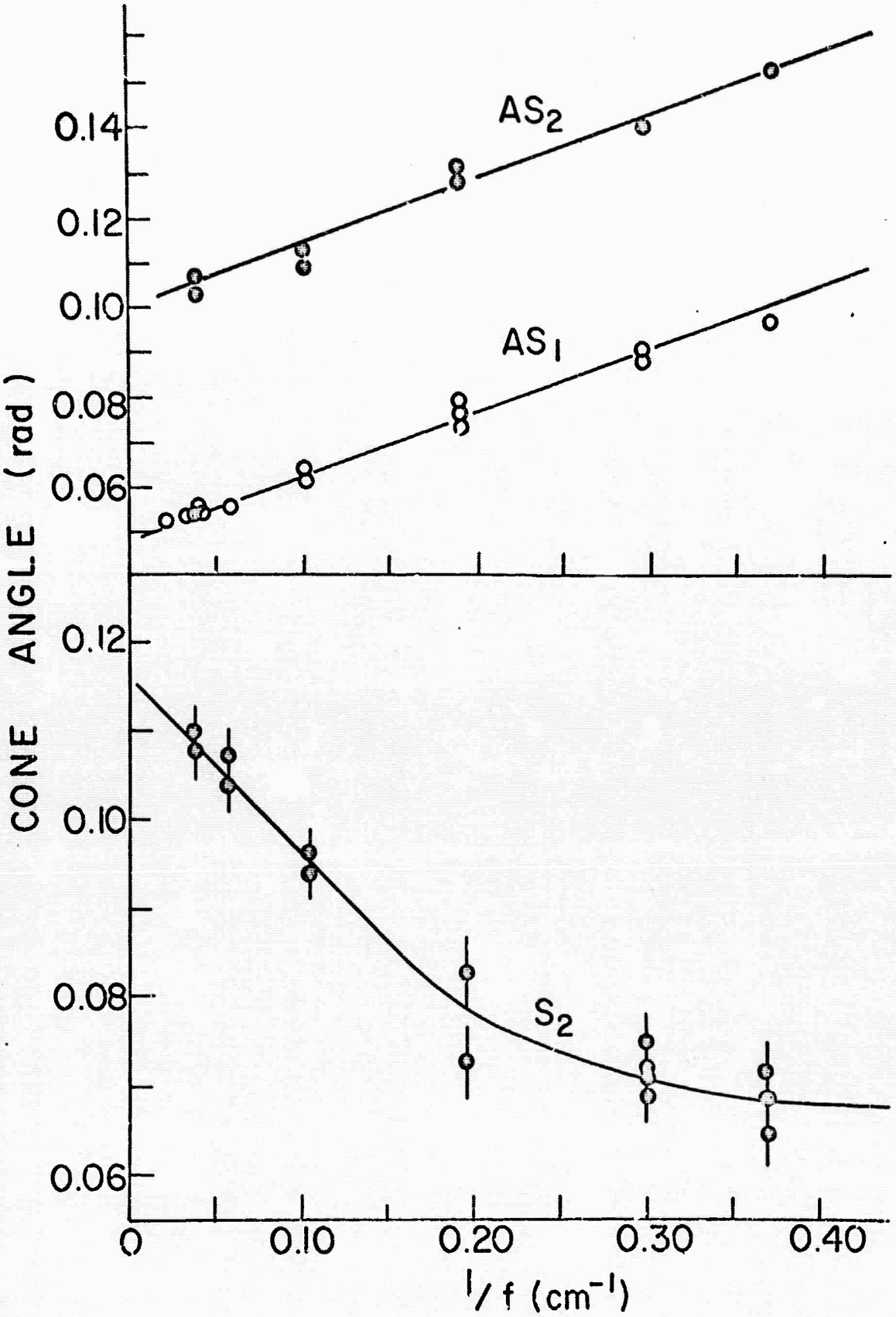
0.14
0.12
0.10
0.08
0.06
AS2
AS1
CONE ANGLE (rad)
0.12
0.10
0.08
0.06
S2
0
0.10
0.20
0.30
0.40
1/f (cm-1)

FIG. 6.

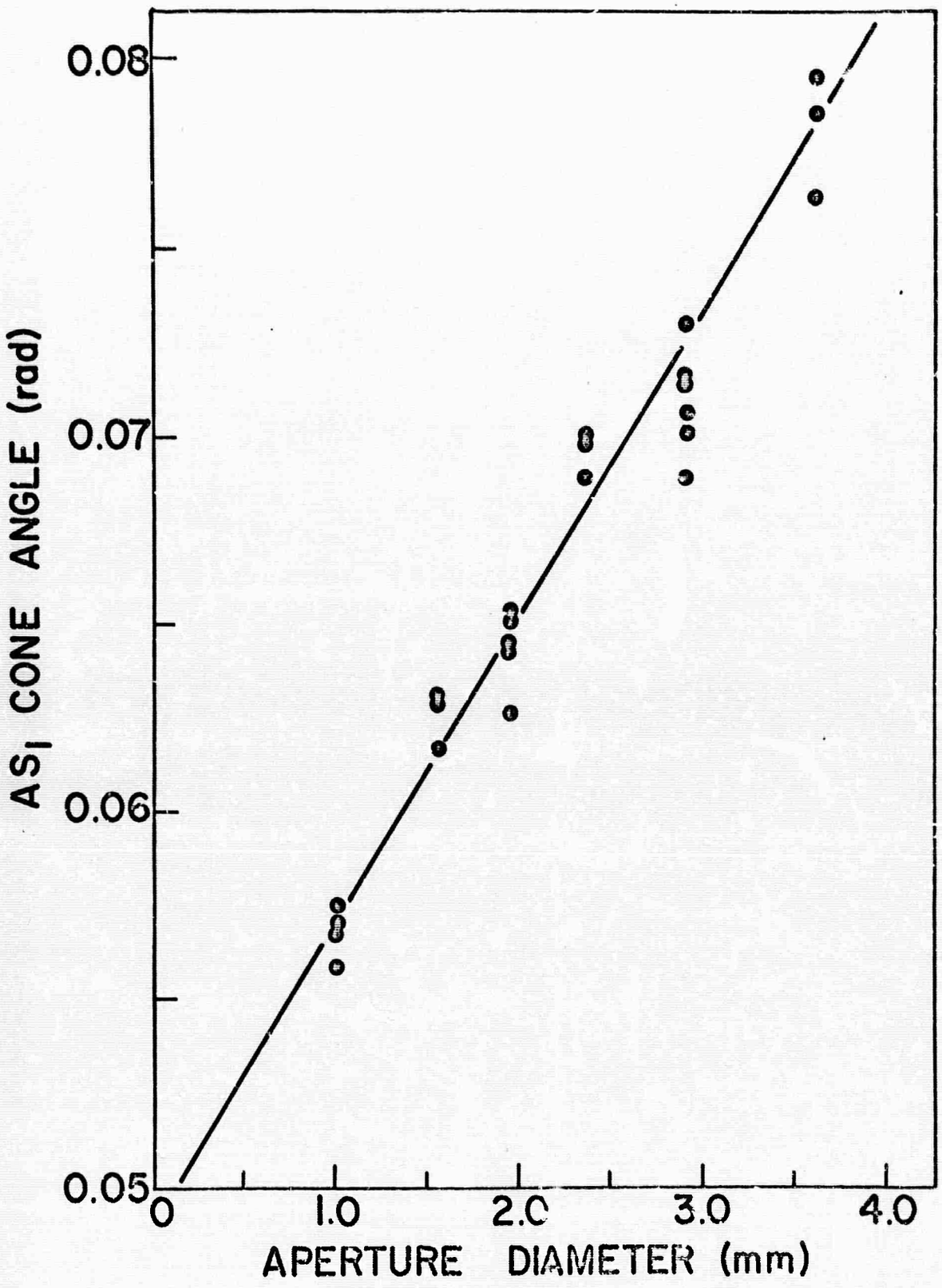
0.08
0.07
0.06
0.05
AS$_1$ CONE ANGLE (rad)
0
1.0
2.0
3.0
4.0
APERTURE DIAMETER (mm)

FIG. 7.

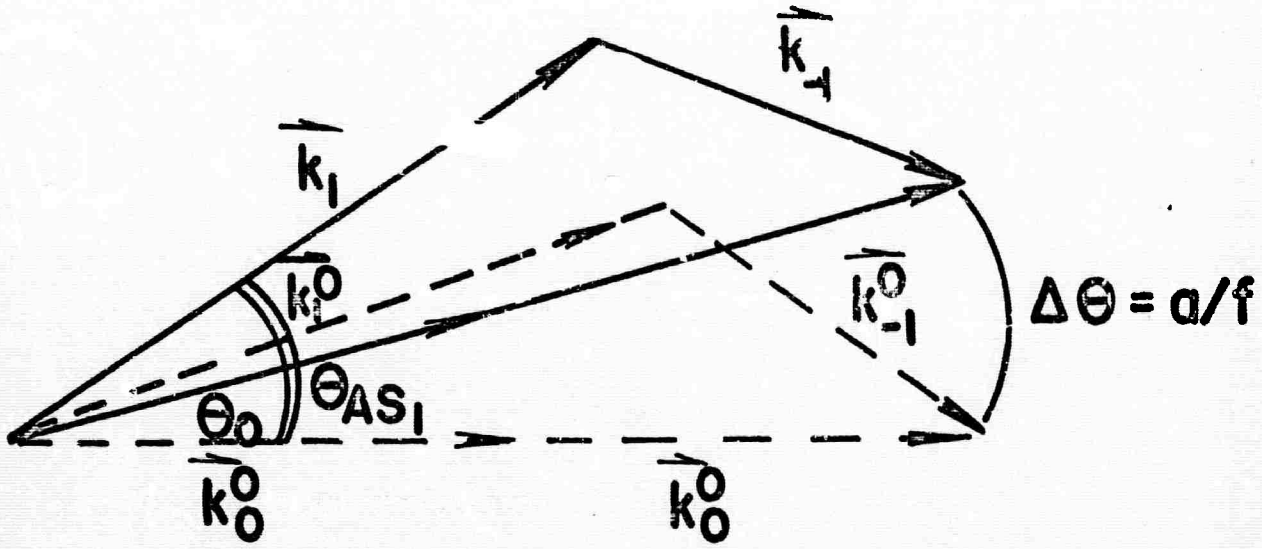
$\vec{k}_{-1}$
$\vec{k}_1$
$\vec{k}_1^o$
$\vec{k}_{-1}^o$
$\Delta\Theta = a/f$
Θ_o
Θ_{AS_1}
$\vec{k}_o^o$
$\vec{k}_o^o$

(a)

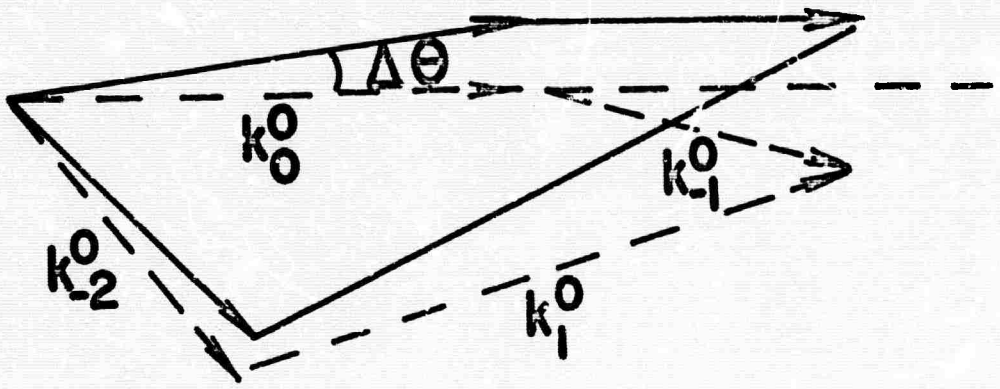
$\Delta\Theta$
$\vec{k}_o^o$
$\vec{k}_{-1}^o$
$\vec{k}_{-2}^o$
$\vec{k}_1^o$

(b)

FIG. 8.

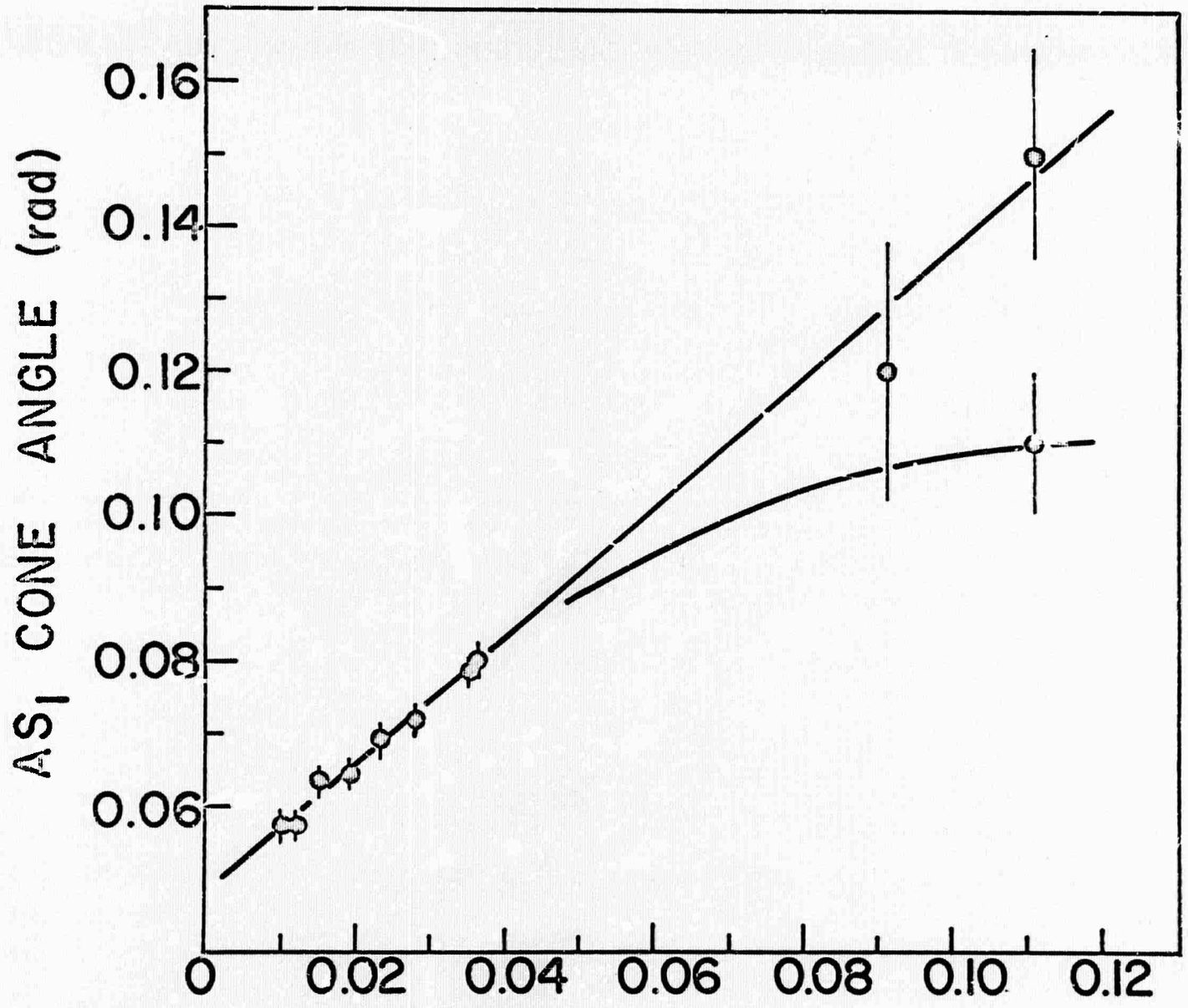
0.16
0.14
0.12
0.10
0.08
0.06
AS1 CONE ANGLE (rad)
0
0.02
0.04
0.06
0.08
0.10
0.12
APERTURE RATIO a / f

FIG. 9.

FIG. 10.

High-Speed Spectroscopy Using the Inverse Raman Effect.*

R.A. McLaren† and B.P. Stoicheff

Department of Physics, University of Toronto

Toronto 181, Canada

'RACT

A method of obtaining inverse Raman spectra over the range of frequency shifts ~ 300 to 3500 cm^{-1} in liquids and solids in a time of ~ 40 nsec is described. The stimulating monochromatic radiation at 6940 Å is provided by a giant-pulse ruby laser; the background continuum is the short-lived spontaneous fluorescence of rhodamine B or 6G excited by second-harmonic radiation (3470 Å) produced in KDP from a small part of the main laser beam, thus ensuring simultaneous irradiation of the sample by both beams.

*This research is part of Project DEFENDER under the joint sponsorship of the Advanced Research Projects Agency, the U.S. Office of Naval Research, and the Department of Defense. Also supported by the National Research Council, Canada, and the University of Toronto.

†Holder of a National Research Council of Canada Scholarship 1968-69.

When a molecular medium is irradiated simultaneously by intense monochromatic light at frequency ν_L, and by a continuum of higher frequencies, absorption occurs from the continuum at frequencies $\nu_L + \nu_M$ where ν_M is a Raman frequency of the medium. This phenomenon, known as the inverse Raman effect has been reported by a number of authors[1-4]; but its usefulness has been severely limited by the lack of a suitable source of continuum. In order to observe this effect, a high electric field at frequency ν_L is required, such as that produced by a giant-pulse ruby laser. In addition, the continuum and the laser pulse must be coincident as they pass through the scattering medium; and, for photographic detection, the continuum must last no longer than the laser pulse. A good continuum must be broad enough to cover a wide range of Raman frequencies ν_M, and sufficiently intense to be detectable despite its short duration.

Previous authors have used broad stimulated anti-Stokes Raman emission[1,2,3] and sparks[4] as continuum sources, but neither of these has proved completely satisfactory. This Letter reports the use of two fluorescing organic dyes, rhodamine 6G (2.0×10^{-3} M in methanol) and rhodamine B (2.0×10^{-3} M in ethanol) as continuum sources. Both of these dyes absorb very strongly at 3470 Å, the second harmonic of the ruby laser emission, and both have intense fluorescence bands extending from $\sim$ 5600 Å to $\sim$ 6800 Å. This is sufficient spectral breadth to cover Raman shifts from 300 cm^{-1} to 3500 cm^{-1} when the stimulating radiation is the ruby laser emission at 6940 Å. The fluorescence lifetime of rhodamine 6G has been reported as 5.5 nsec[5], sufficiently short to provide good

coincidence with the laser pulse.

The experimental arrangement is shown in Fig. 1. A ruby laser Q-switched by a rotating prism produced the stimulating radiation at ν_L in a single pulse with full-width at half-maximum of $\sim$ 40 nsec and with energy equal to $\sim$ 0.30 joules. Approximately 3% of the laser emission was converted to $2\nu_L$ in a crystal of phase-matched KDP. Radiation at ν_L and $2\nu_L$ was then separated into two beams[6] by a glass prism. The 3470 Å radiation was incident upon a 1 mm thickness of dye solution contained in a glass cell. The resulting normal fluorescence continuum along with the laser beam ν_L was then trapped by total internal reflection in a glass capillary cell containing the scattering liquid. This ensured spatial coincidence between the stimulating radiation and the continuum. The capillary cell had inner and outer diameters of 2.4 mm and 4.0 mm respectively, and was 15 cm long; the electric field inside the capillary was estimated to be $\sim 1.2 \times 10^5$ V/cm. The exit end of the cell was imaged on the slit of a grating spectrograph having a dispersion of 10 Å/mm. Spectra were recorded on Kodak IF photographic plates and on Polaroid film. With a slit width of 100 μ, the intensity of the background continuum at larger frequency shifts was sufficient to record spectra in a single laser pulse; however in the region of smaller frequency shifts (i.e. longer wavelengths) several pulses were required to accumulate sufficient continuum intensity.

Inverse Raman spectra of diamond and of liquid benzene and toluene have been photographed using the above technique and are shown in Figs. 2 and 3. In Fig. 2a is shown the spectrum of the

continuum alone after passing through a 15 cm path length of benzene; in Fig. 2b is shown the spectrum obtained when both monochromatic and continuum beams traverse the benzene sample. It should be noted that several weak vibrational bands are readily observed, in addition to the intense "C-H stretching" band (which is the only one observed in this region in stimulated Raman emission). Since the same matrix elements of the polarizability are involved in the inverse Raman effect as in normal Raman emission, the same selection rules relating to the state of polarization of the incident and scattered radiation apply. This is demonstrated qualitatively in Fig. 2c which shows the effect of various states of polarization of the monochromatic and continuum radiation on the appearance of the strongly polarized line at 3062 cm^{-1} and its depolarized neighbour at 3047 cm^{-1}. The laser emission ν_L was plane polarized. In the upper spectrum the continuum was unpolarized; the 3062 cm^{-1} absorption line is strong while the 3047 cm^{-1} line slightly to the right of it is extremely weak. In the middle spectrum, the continuum has been polarized perpendicular to the laser polarization; the 3062 cm^{-1} absorption is much weaker appearing equal to that at 3047 cm^{-1}. In the bottom spectrum the continuum has been polarized parallel to the laser polarization; only the 3062 cm^{-1} line appears. In Fig. 3 are shown the spectra of benzene and toluene in the region of the "C-C stretching" bands, and in addition the sharp band at 1332 cm^{-1} of diamond obtained from a cross-sectional area of $\sim 5 \times 10^{-2}$ cm^2 of a crystal 2.4 mm thick.

The use of fluorescing organic dyes as sources of continuum

has made it possible to photograph Raman spectra covering a wide range of molecular frequencies in a time of 40 nsec. Such spectra may be useful in the study of short-lived molecular species and of transient phenomena, including for example, Stark and Zeeman effects in pulsed electric and magnetic fields. It should be possible to reduce the time to the subnanosecond range and perhaps to $\sim$30 psec (and still obtain a resolution of $\sim$1 cm^{-1}) by using mode-locked lasers to produce the stimulating radiation. This would, of course, necessitate an equally short-duration continuum of high intensity, perhaps produced by a mode-locked dye laser.

REFERENCES

1. W.J. Jones and B.P. Stoicheff, Phys. Rev. Letters 13, 657 (1964).

2. A.K. MacQuillan and B.P. Stoicheff, Physics of Quantum Electronics, ed. by P.L. Kelley, B. Lax, P.E. Tannenwald; McGraw-Hill Book Company, New York (1966), p. 192.

3. J.A. Duardo, F.M. Johnson and M.A. El-Sayed, Phys. Letters 21, 168 (1966).

4. S. Dumartin, B. Oksengorn and B. Vodar, Comptes rendus 261, 3767 (1965).

5. A.J. DeMaria, private communication (1968).

6. In preliminary attempts to produce inverse Raman spectra the beams were not separated and both beams were incident on the dye cell. However, the presence in the dye cell of the intense field at ν_L greatly reduced the intensity of the normal fluorescence making this simple geometry impractical. The mechanism responsible for this effect is not understood.

FIGURE CAPTIONS

Fig. 1. A schematic diagram of the apparatus.

Fig. 2. Inverse Raman spectrum of liquid benzene in the region of the C-H stretching vibration.

(a) continuum after traversing a 15 cm length of benzene. (b) spectrum obtained when monochromatic beam at ν_L and continuum traverse the liquid. (c) spectra obtained when continuum is unpolarized (upper), polarized perpendicular to laser beam (middle) and polarized parallel to laser beam (lower).

Fig. 3. Inverse Raman spectra of diamond, and liquid toluene and benzene in the region of the C-C stretching vibrations.

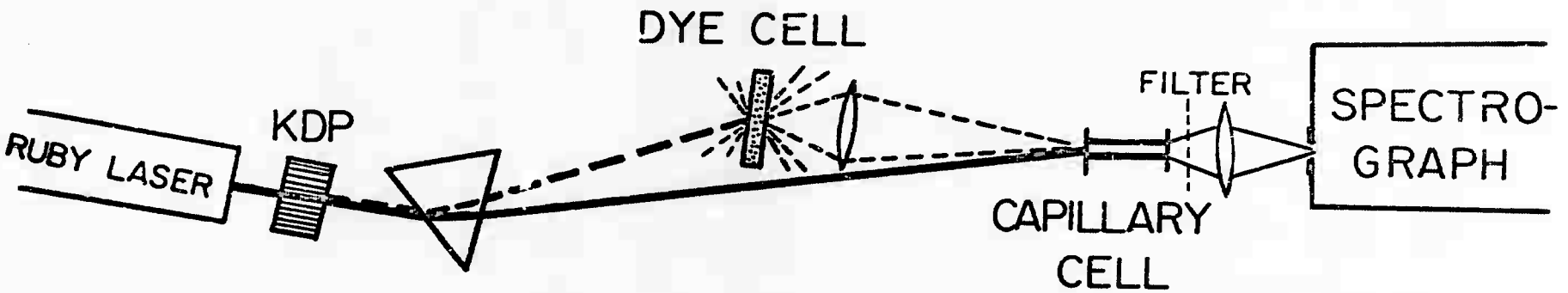

FIG. 1. McLAREN & STRICKOFF

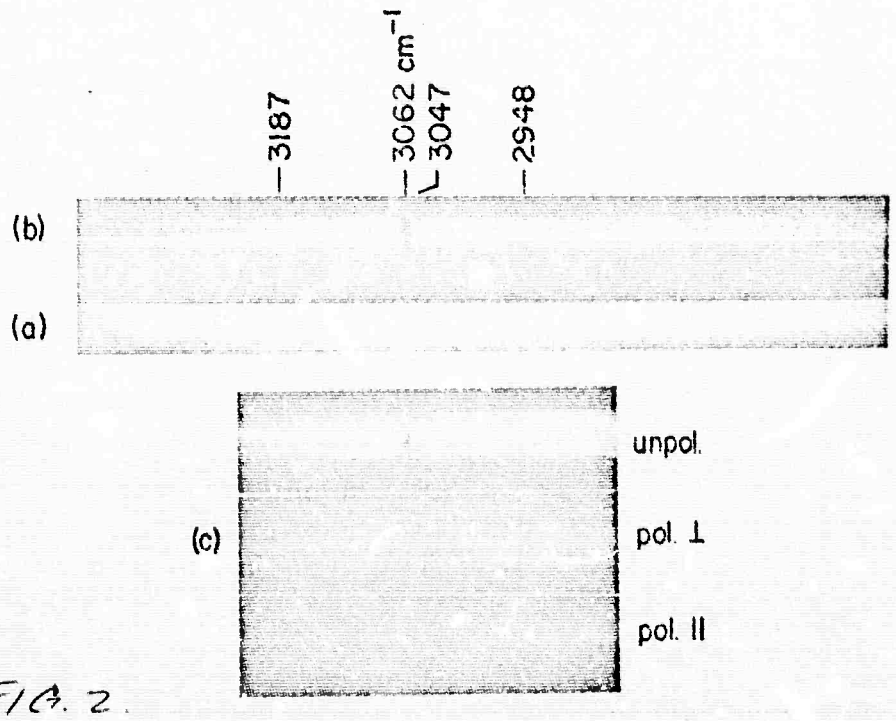

FIG. 2.

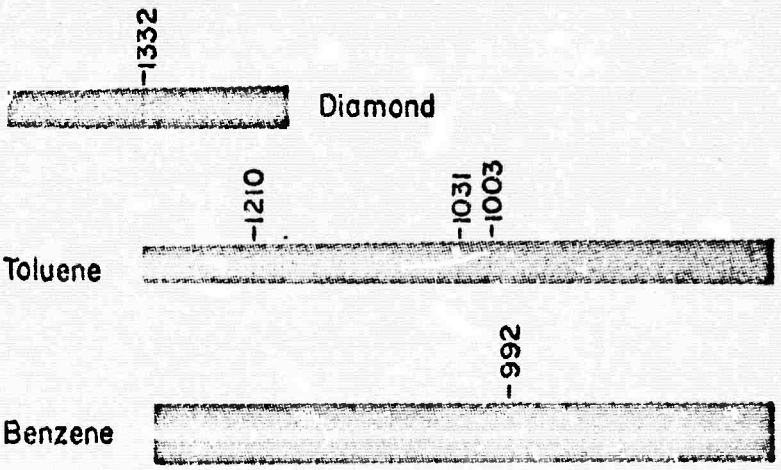

FIG 3. Nelson + Stockli.

Unclassified

Security Classification

DOCUMENT CONTROL DATA - R&D

(Security classification of title, body of abstract and indexing annotation must be entered when the overall report is classified)

1. ORIGINATING ACTIVITY *(Corporate author)*

Department of Physics
University of Toronto
TORONTO 5, Ontario

2a. REPORT SECURITY CLASSIFICATION

Unclassified

2b. GROUP

3. REPORT TITLE

Stimulated Raman Emission and Absorption Spectroscopy

4. DESCRIPTIVE NOTES *(Type of report and inclusive dates)*

Final Report 1 June 1965 - 31 August 1969

5. AUTHOR(S) *(Last name, first name, initial)*

Stoicheff, Boris P. Clements, Wallace R.L. McLaren, Robert A.
Shimizu, Fujio Bachmann, Urs
McQuillan, Archie K. Grun, Bernard J.

6. REPORT DATE	7a. TOTAL NO. OF PAGES	7b. NO. OF REFS
November 1969	77	110

8a. CONTRACT OR GRANT NO.	9a. ORIGINATOR'S REPORT NUMBER(S)
Nonr-5012(00)	No. 8
b. PROJECT NO. NR 015-813/4-14-65	
c. Authorization ARPA Order No. 306	9b. OTHER REPORT NO(S) *(Any other numbers that may be assigned this report)*
d.	

10. AVAILABILITY/LIMITATION NOTICES

Distribution of this document is unlimited.

11. SUPPLEMENTARY NOTES	12. SPONSORING MILITARY ACTIVITY
	Office of Naval Research, and Advanced Research Projects Agency

13. ABSTRACT

1. "Frequency Broadening in Liquids by a Short Light Pulse".
2. "Angular Distribution of Surface Radiation in Stimulated Raman Scattering".
3. "Raman Linewidths for Stimulated Threshold and Gain Calculations".
4. "Intensity and Gain Measurements on the Stimulated Raman Emission in Liquid O_2 and N_2".
5. "A Study of the Duration and Birefringence of Self-Trapped Filaments in CS_2".
6. "High-Resolution Raman Spectroscopy of Gases with Laser Excitation".
7. "Stimulated Raman Emission in Diamond: Spectrum, Gain and Angular Distribution of Intensity".
8. "High-Speed Spectroscopy Using the Inverse Raman Effect".

DD FORM 1473

Unclassified

14. KEY WORDS	LINK A		LINK B		LINK C	
	ROLE	WT	ROLE	WT	ROLE	WT
Stimulated Raman Emission						
Stimulated Raman Absorption						
Angular Distribution of Raman Radiation						
Properties of Filaments						
High-Resolution Raman Spectroscopy						
High-Speed Raman Spectroscopy						
Raman Linewidth Measurements						

INSTRUCTIONS

1. ORIGINATING ACTIVITY: Enter the name and address of the contractor, subcontractor, grantee, Department of Defense activity or other organization *(corporate author)* issuing the report.

2a. REPORT SECURITY CLASSIFICATION: Enter the overall security classification of the report. Indicate whether "Restricted Data" is included. Marking is to be in accordance with appropriate security regulations.

2b. GROUP: Automatic downgrading is specified in DoD Directive 5200.10 and Armed Forces Industrial Manual. Enter the group number. Also, when applicable, show that optional markings have been used for Group 3 and Group 4 as authorized.

3. REPORT TITLE: Enter the complete report title in all capital letters. Titles in all cases should be unclassified. If a meaningful title cannot be selected without classification, show title classification in all capitals in parenthesis immediately following the title.

4. DESCRIPTIVE NOTES: If appropriate, enter the type of report, e.g., interim, progress, summary, annual, or final. Give the inclusive dates when a specific reporting period is covered.

5. AUTHOR(S): Enter the name(s) of author(s) as shown on or in the report. Enter last name, first name, middle initial. If military, show rank and branch of service. The name of the principal author is an absolute minimum requirement.

6. REPORT DATE: Enter the date of the report as day, month, year, or month, year. If more than one date appears on the report, use date of publication.

7a. TOTAL NUMBER OF PAGES: The total page count should follow normal pagination procedures, i.e., enter the number of pages containing information.

7b. NUMBER OF REFERENCES: Enter the total number of references cited in the report.

8a. CONTRACT OR GRANT NUMBER: If appropriate, enter the applicable number of the contract or grant under which the report was written.

8b, 8c, & 8d. PROJECT NUMBER: Enter the appropriate military department identification, such as project number, subproject number, system numbers, task number, etc.

9a. ORIGINATOR'S REPORT NUMBER(S): Enter the official report number by which the document will be identified and controlled by the originating activity. This number must be unique to this report.

9b. OTHER REPORT NUMBER(S): If the report has been assigned any other report numbers *(either by the originator or by the sponsor)*, also enter this number(s).

10. AVAILABILITY/LIMITATION NOTICES: Enter any limitations on further dissemination of the report, other than those imposed by security classification, using standard statements such as:

(1) "Qualified requesters may obtain copies of this report from DDC."

(2) "Foreign announcement and dissemination of this report by DDC is not authorized."

(3) "U. S. Government agencies may obtain copies of this report directly from DDC. Other qualified DDC users shall request through _____."

(4) "U. S. military agencies may obtain copies of this report directly from DDC. Other qualified users shall request through _____."

(5) "All distribution of this report is controlled. Qualified DDC users shall request through _____."

If the report has been furnished to the Office of Technical Services, Department of Commerce, for sale to the public, indicate this fact and enter the price, if known.

11. SUPPLEMENTARY NOTES: Use for additional explanatory notes.

12. SPONSORING MILITARY ACTIVITY: Enter the name of the departmental project office or laboratory sponsoring *(paying for)* the research and development. Include address.

13. ABSTRACT: Enter an abstract giving a brief and factual summary of the document indicative of the report, even though it may also appear elsewhere in the body of the technical report. If additional space is required, a continuation sheet shall be attached.

It is highly desirable that the abstract of classified reports be unclassified. Each paragraph of the abstract shall end with an indication of the military security classification of the information in the paragraph, represented as *(TS)*, *(S)*, *(C)*, or *(U)*.

There is no limitation on the length of the abstract. However, the suggested length is from 150 to 225 words.

14. KEY WORDS: Key words are technically meaningful terms or short phrases that characterize a report and may be used as index entries for cataloging the report. Key words must be selected so that no security classification is required. Identifiers, such as equipment model designation, trade name, military project code name, geographic location, may be used as key words but will be followed by an indication of technical context. The assignment of links, roles, and weights is optional.